WINGED ROCKET PERFORMANCE ANALYSIS

Thesis by

David E. Shonerd

In Partial Fulfillment of the Requirements

For the Degree of

Aeronautical Engineer

Jet Propulsion

California Institute of Technology

Pasadena, California

1949

ACKNOWLEDGMENTS

The writer is deeply indebted to Mr. Henry Nagamatsu for his continued interest and helpfulness during this investigation. Invaluable assistance was also rendered by Miss Laura Andrews and Mrs. Melba Nead in computing trajectories and by Miss Patricia Line in typing and assembling the final manuscript.

ABSTRACT

A method is presented for estimating the effects of various parameters on the performance of a winged rocket. A program for studying three specific parameters, i.e., wing areas, reduced thrust cruising programs, and trajectory climb angles, and their effect on the horizontal range of a winged rocket is presented. Complete calculations are carried out for one combination of these parameters.

An analysis of the Lift, Drag and Stability characteristics of a long, slender rocket with trapezoidal fins and wings is made. The stabilizing effectiveness of delta and trapezoidal fins is compared.

Simplified approximate methods of integrating the trajectory equations by step-by-step method are presented.

TABLE OF CONTENTS

LIST OF TABLES

LIST OF FIGURES

LIST OF FIGURES - (continued)

LIST OF SYMBOLS

A Body cross-sectional area (ft^2)

a Missile acceleration along flight path (ft/sec^2)

a_o Speed of sound (ft/sec)

C_D Drag coefficient

C_{D_i} Coefficient of induced drag

C_{D_f} Coefficient of skin friction drag

C_{D_o} Coefficient of parasite drag

C_{D_N} Coefficient of nose wave drag

C_F Thrust coefficient

C_L Coefficient of lift

C_{L_W} Coefficient of wing lift

c Wing or tail chord length (ft)

D Drag force (lbs)

d Rocket diameter (ft)

F Thrust (lbs)

F_V Velocity thrust (lbs)

f_e Nozzle exit area (in^2)

f_t Nozzle throat area (in^2)

g Acceleration due to gravity (ft/sec^2)

I Total impulse (lb secs)

I_{SP} Specific impulse (secs)

K Effectiveness factor

L Lift force (lbs)

LIST OF SYMBOLS (continued)

L''	Preliminary value of missile lift computed for $\frac{d\theta}{dt}$ equal to zero (lbs)
ℓ_{CP}	Distance from base of rocket to center of pressure (ft)
ℓ_{CG}	Distance from base of rocket to center of gravity (ft)
ℓ_N	Distance from base of rocket to nose lift vector (ft)
ℓ_T	Distance from base of rocket to tail lift vector (ft)
ℓ_W	Distance from base of rocket to wing lift vector (ft)
M	Free stream Mach number
P_B	Body base pressure (lb/ft^2)
P_C	Rocket chamber pressure (lb/in^2)
P_e	Nozzle exit pressure (lb/in^2)
P_o	Atmospheric pressure (lb/in^2)
q	Dynamic pressure, $\frac{1}{2} \rho V^2$ (lb/ft^2)
R	Radius of the earth (ft)
S_W	Wing area (ft^2)
t	Time (secs)
t_p	Burning time of propellant (secs)
t_W	Wing thickness (ft)
V_e	Rocket effective exhaust velocity (ft/sec)
W	Weight of rocket (lbs)
W_o	Initial gross weight of rocket (lbs)
W_p	Weight of propellant (lbs)
$\dot{W}_p$	Burning rate of propellant (lbs/sec)

LIST OF SYMBOLS (continued)

x	Horizontal coordinate in trajectory (ft)
y	Vertical coordinate in trajectory (ft)
α	Rocket angle of attack (degrees)
α_w	Wing angle of attack (degrees)
ϵ	Nozzle area ratio,
θ	Angle of trajectory relative to horizontal (degrees)
θ_s	Cone half angle of body (degrees)
μ	Ratio of gross weight to cross-sectional area (lb/ft^2)
ν	Ratio of propellant weight to gross weight
ρ	Air density ($slug/ft^3$)
ρ_0	Sea level air density ($slug/ft^3$)
σ	Ratio of air density at altitude to sea level air density
$()_B$	Relative to body
$()_T$	Relative to tail
$()_W$	Relative to wing
$()_N$	Relative to nose
$()_S$	Values at summit of trajectory
$()_P$	Values at end of burning

I. INTRODUCTION

An analysis of the general performance problem of a winged rocket must consider separately each of the many parameters which will effect the horizontal range, speed and altitude of the rocket. Three of these factors were investigated in this study. With other conditions fixed, wing areas, reduced thrust cruising periods, and trajectory climb angles were varied; their effects on the horizontal range of a missile of the type shown in Fig. 1 were considered.

The general flight problem of winged rockets is becoming of increasing importance as more of the questions associated with the sounding rocket performance are being answered (Cf. Ref. 1). The number of parameters of interest increases manyfold when a vertical trajectory is changed into one of the many possible types of inclined trajectories, and when a vehicle which uses aerodynamic forces only for stability is changed into a vehicle which uses aerodynamic forces to sustain flight.

One type of rocket is considered in this investigation (Cf. Fig. 1 and Table I). It has a long, slender, round body with a conical nose and trapezoidal shaped fins and wings. It is assumed to have sufficient control effectiveness to approximate the types of trajectories investigated. Principle aerodynamic control is achieved through changing of the wing angle of attack.

This investigation was resolved into two parts. First, an analysis of the variables of rocket aerodynamics, rocket thrust and trajectory was made. Second, these variables were used in step-by-step integrations over trajectories to determine the effects of the variable parameters under

discussion. Accordingly, this report of the investigation is divided into the individual analyses of trajectory, missile aerodynamic properties, and trajectory calculation procedure, and finally the conclusions reached.

The following general assumptions were made in this study:

1) Aerodynamic properties at very high Mach numbers (4 to 8) may either be calculated by linearized theory, or may be obtained by extrapolation of results obtained for lower Mach numbers.

2) Modifications to conventional supersonic theory due to rarified gases may be neglected.

3) Atmospheric properties are as specified in the NACA Standard Atmosphere (Cf. Refs. 2 and 3).

4) The problems associated with the aerodynamic heating of the rocket will not be considered.

5) Possible limitations caused by structural or control problems will not be considered.

Other specific assumptions and approximations are discussed in the sections following.

II. TRAJECTORY CONSIDERATIONS

A rocket trajectory can be logically separated into three parts, i.e., the launching phase, the powered phase, and the gliding or ballistic phase (Cf. Fig. 2). The launching phase has important problems in low speed stability and in complexity of launching equipment required. The powered portion of the flight must be oriented so as to convert as much as possible of the power plant energy into usable kinetic and potential energy of the rocket. The glide or ballistic part of the trajectory must be established to convert rocket energy into the longest possible horizontal range.

The calculations of vertical vacuum trajectories give performance data which are useful in the preliminary estimates of design conditions. Values of μ, the ratio of gross weight to rocket cross-sectional area, indicate how closely the vertical vacuum trajectory of a wingless rocket will correspond to an actual trajectory; for high values of μ, the drag effect in an atmospheric trajectory is small. Since the values of μ for these configurations are approximately 3,000 (Cf. Table I), the drag effect for a wingless vehicle would be small. With wings, however, a vacuum trajectory may vary appreciably from an actual trajectory.

A vacuum trajectory for the sea level thrust conditions of Case I (Cf. Table II) was computed. It approximates the conditions existing during a vertical launching phase and indicates the order of magnitude of the Mach numbers to be achieved at the end of propellant burning. The following equations were used:

$$y = \frac{V_e t_p}{v}\left(1 - v\frac{t}{t_p}\right)\log\left(1 - v\frac{t}{t_p}\right) + V_e t - \frac{1}{2}gt^2$$

$$\frac{dy}{dt} = -V_e \log\left(1 - v\frac{t}{t_p}\right) - gt$$

where y = vertical coordinate

V_e = effective exhaust velocity

The following results were obtained for V_e equal to 6,440 feet per second, v equal to 0.7 and t_p equal to 40 seconds:

After ten seconds of flight:

Altitude = 5,800 ft.

Velocity = 900 ft./sec.

Mach number = 0.8

After 40 seconds of flight:

Altitude = 121,700 ft.

Velocity = 6,440 ft./sec.

Mach number = 6.1

At the summit of vacuum trajectory:

Time = 240 sec.

Altitude = 766,000 ft.

This data differs from the actual trajectory data by the magnitude of the drag term and the effect of increase of thrust with altitude.

A vertical launching phase will be assumed for all trajectories. Launching and equipment required for rockets of the size of these configurations is simple for vertical flight, but becomes complex for launching angles tilted from the vertical. Vertical flight will be maintained until sufficient velocity is attained to give, first, adequate stability and, second, the control effectiveness required for changing the flight path angle and, third, sufficient aerodynamic lifting forces to hold the rocket on a non-vertical flight path. Data from the vacuum trajectory indicates

that a flight time of 10 seconds will be sufficient for the boost phase of all trajectories. The high burning rate of propellant of Case I will be used during this initial launching period.

The second phase of the trajectory has its objective in positioning the rocket for an optimum coasting path with a minimum expenditure of energy. Energy is absorbed during the powered flight by drag forces, propellant inertial forces and inertial forces of the rocket empty weight. The position of the rocket for an optimum coasting trajectory is dependent on the aerodynamic characteristics of the vehicle but generally must be within the atmosphere (Cf. Ref. 5).

Each of the sources of energy absorption during the powered trajectory may be minimized by proper choice of thrust and flight program. The requirements are contradictory, however, and an optimum solution represents a balance of compensating effects. The drag forces are a minimum for the shortest paths and lowest velocities in the atmosphere. The propellant inertial forces are a minimum for the most rapid burning rate of the propellant; this results in highest velocities at relatively low altitudes. Effects of inertial forces due to rocket empty weight are minimized in the vacuum trajectory case for angles of the flight path inclined initially at 45 degrees to the horizontal.

Three trajectory angles, θ, of 20, 40, and 60 degrees relative to the horizontal will establish the influence of this factor on rocket horizontal range. The vehicle can be maintained on a constant climb angle trajectory by appropriate control of the aerodynamic surfaces.

The third portion of the trajectory is identified by zero thrust from the rocket motor. If the rocket is above the atmosphere, the trajectory

is ballistic. If the rocket is in the atmosphere, the trajectory is some type of a free or controlled glide path. It is assumed in this investigation that the vehicle glides at maximum lift-drag ratio for this portion of the trajectory.

Dr. Walther (Cf. Ref. 5) discusses the oscillations which occur in a maximum lift-drag ratio glide if the glide path is not begun at an altitude for which the aerodynamic forces are in equilibrium at a constant glide angle. If the rocket is too high at the beginning of the glide, it will drop rapidly into denser air and approach a constant glide angle in an oscillatory manner. It was concluded that maximum range would be obtained by controlling the vehicle so that it begins the glide at maximum lift-drag ratio after as few oscillations as possible.

The following assumptions are made with regard to the three phases of the trajectory:

1) No energy loss occurs in turning from the vertical launching path to the inclined climb path.

2) The change from initial thrust to reduced thrust occurs instantaneously.

3) The rocket maintains zero angle of attack relative to the flight path through proper controls. Variation of aerodynamic lift is obtained by varying the incidence angle of the wing.

4) Wing angles of attack are limited to the values required for maximum lift-drag ratio at a Mach number of 8.0.

III. STABILITY ANALYSIS

The basic problem of aerodynamic stabilization of a rocket is to maintain the rocket center of pressure behind the center of gravity for all flight Mach numbers. The stabilizing moment is proportional to the distance between the center of gravity and center of pressure locations. In general it should be relatively small since the control apparatus must overcome this moment for maneuvering. Accordingly, it is desirable to have a center of pressure which remains in a fixed position a short distance behind the center of gravity.

The stability analysis established a rocket configuration which was stable up to the highest Mach number determined in the vacuum trajectories, i.e., a Mach number of 6.0. The rocket center of gravity position was assumed constant during the trajectory since a complete weight analysis would be necessary for a more accurate determination of center of gravity location. Wing and fin planforms were selected after comparing the stabilizing effectiveness of delta and trapezoidal planforms. A final determination of center of pressure travel for all flight Mach numbers was made for each of the vehicle configurations.

Selection of fin and wing planforms was based on the considerations of lift-drag ratio, weight of structure, center of pressure movement with Mach number and areas required to give positive stability and design lift. As a first step in the selection of fin and wing planforms, a study was made of the fin areas required to give positive stability of 0.5 caliber for Mach numbers as high as 6.0. Two fin planforms were compared by writing the stability equation for a rocket at a small angle of attack. The forces

acting on a rocket and the planforms considered are shown in Figs. 3 and 4. The stability equation is

$$P_N \ell_N + P_T \ell_T = (P_N + P_T) \ell_{c.p.} \qquad (1)$$

or

$$\left(\frac{dC_L}{d\alpha}\right)_N \alpha q d^2 \ell_N + \left(\frac{dC_L}{d\alpha}\right)_T \alpha q d^2 \ell_T = \left[\left(\frac{dC_L}{d\alpha}\right)_N + \left(\frac{dC_L}{d\alpha}\right)_T\right] \alpha q d^2 \ell_{c.p.}$$

simplifying

$$\left(\frac{dC_L}{d\alpha}\right)_N \ell_N + \left(\frac{dC_L}{d\alpha}\right)_T \ell_T = \left[\left(\frac{dC_L}{d\alpha}\right)_N + \left(\frac{dC_L}{d\alpha}\right)_T\right] \ell_{c.p.} \qquad (2)$$

Rocket stability is indicated by the relation between $\ell_{c.g.}$ and $\ell_{c.p.}$. For positive stability, $\ell_{c.p.}$ must be less than $\ell_{c.g.}$. Equation (2) may be expressed in terms of Mach number and fin area in the following manner:

$\left(\frac{dC_L}{d\alpha}\right)_N =$ F_N (Mach) (Cf. Fig. 7)

$\left(\frac{dC_L}{d\alpha}\right)_T = \frac{4}{\sqrt{M^2-1}}$ for planform 2

$\left(\frac{dC_L}{d\alpha}\right)_T =$ F_N (Mach) (Cf. Fig. 6), for planform 1

$\ell_N =$ 35 feet assuming the nose lift acts at the tip

$\ell_T = \frac{1}{3} C_{R_1}$ for planform 1

$\ell_T = .55\, C_{R_2}$ for planform 2

$\ell_{c.g.} =$ 14.7 feet (Cf. Table I)

$$\ell_{c.p.} = \ell_{c.g} - \tfrac{1}{2} \text{ caliber}$$

$$= 13.4 \text{ feet}$$

$$C_{R_1}^2 = 3.7\, S_{T_1}$$

$$C_{R_2}^2 = 0.93\, S_{T_2}$$

Equation (2) becomes, after substitution:

For Planform 1:

$$35\left(\frac{dC_L}{d\alpha}\right)_N + \frac{1}{3} C_{R_1} \frac{S_{T_1}}{d^2}\left(\frac{dC_L}{d\alpha}\right)_T = \left[\left(\frac{dC_L}{d\alpha}\right)_N + \left(\frac{dC_L}{d\alpha}\right)_T \frac{S_{T_1}}{d^2}\right] 13.4$$

Simplifying:

$$S_{T_1}\sqrt{S_{T_1}} - 20.9\, S_{T_1} + 209 \left(\frac{dC_L}{d\alpha}\right)_N \Big/ \left(\frac{dC_L}{d\alpha}\right)_T = 0 \qquad (3)$$

For Planform 2:

$$35\left(\frac{dC_L}{d\alpha}\right)_N + \frac{4}{\sqrt{M^2-1}} \frac{S_{T_2}}{d^2} \times .55 C_{R_2} = \left[\left(\frac{dC_L}{d\alpha}\right)_N + \frac{4}{\sqrt{M^2-1}} \frac{S_{T_2}}{d^2}\right] 13.4$$

Simplifying:

$$S_{T_2}\sqrt{S_{T_2}} - 25.3\, S_{T_2} + 63.5\sqrt{M^2-1}\left(\frac{dC_L}{d\alpha}\right)_N = 0 \qquad (4)$$

Equations (3) and (4) are plotted in Figure 4 as the fin area required for stability with no body effects considered.

The effectiveness of the delta wing is increased greatly if the body lift effects are considered. Spreiter has outlined a method (Cf. Ref. 6) whereby body effect can be included by use of an effectiveness factor such that:

$$\left(\frac{dC_L}{d\alpha}\right)_{FIN+BODY} = K\left(\frac{dC_L}{d\alpha}\right)_{FIN\ ALONE}.$$

where the projected areas of the fin plus body and fin alone are equal. For fin areas of from 10 to 15 square feet, and for the delta fin planform shown, the values of the effectiveness factor, K, range from 0.85 to 0.88. A constant value of 0.86 was used in this analysis. After corrections are made for reference areas, the equation becomes:

$$\left(\frac{dC_L}{d\alpha}\right)_{FIN+BODY} = 0.86\left(\frac{dC_L}{d\alpha}\right)_{FIN} \times \frac{\text{AREA OF FIN + BODY}}{d^2}$$

$$= 0.66\left(.055 S_T + \sqrt{S_T}\right)\left(\frac{dC_L}{d\alpha}\right)_{FIN\ ALONE} \quad (5)$$

This equation is applicable only to fin plus body configurations which lie well within the Mach cone. Accordingly, for the delta planform under consideration, the results are not reliable beyond a Mach number of 3.0.

The stability equation for planform 1, using the increment of lift due to the body, becomes:

$$S_{T_1}\sqrt{S_{T_1}} - 20.9 S_{T_1} + 317\left[\frac{\left(\frac{dC_L}{d\alpha}\right)_N}{\left(\frac{dC_L}{d\alpha}\right)_T}\right]\left[\frac{1}{\sqrt{S_{T_1}} + .055 S_{T_1}}\right] \quad (6)$$

Solutions to Equation (6) are plotted in Fig. 4.

The trapezoidal fin planform was selected for the final configurations because, first, the comparison indicates that a smaller fin area is required for stability at high Mach numbers, and second, the long root chord required for a delta tail of sufficient area takes up the space on the body that must be used for a wing.

The location of the center of pressure for each of the missile configurations was determined from the stability equations as follows:

$$P_N l_N + P_W l_W + P_T l_T = (P_N + P_W + P_T) l_{c.p.} \qquad (7)$$

or

$$\left(\frac{dC_L}{d\alpha}\right)_N l_N + \left(\frac{dC_L}{d\alpha}\right)_W l_W + \left(\frac{dC_L}{d\alpha}\right)_T l_T = \left[\left(\frac{dC_L}{d\alpha}\right)_N + \left(\frac{dC_L}{d\alpha}\right)_W + \left(\frac{dC_L}{d\alpha}\right)_T\right]$$

Substituting:

$$\frac{4}{\sqrt{M^2-1}} \frac{S_T}{d^2} \times .55^{c}_{R} + \frac{4}{\sqrt{M^2-1}} \frac{S_W}{d^2} 14.7 + \left(\frac{dC_L}{d\alpha}\right)_N \times 35 =$$

$$\left[\frac{4}{\sqrt{M^2-1}} \frac{S_T}{d^2} + \frac{4}{\sqrt{M^2-1}} \frac{S_W}{d^2} + \left(\frac{dC_L}{d\alpha}\right)_N\right] l_{c.p.}$$

Simplifying:

$$S_T \sqrt{S_T} - 25.35 S_T = -63.5 \sqrt{M^2-1} \left(\frac{dC_L}{d\alpha}\right)_N - 2.4 S_W \qquad (8)$$

Equation (8) was first used to establish the fin area required for 0.5 caliber stability at a Mach number of 6.0 for each of the wing areas. Fin areas as shown in Table I were obtained. For these fin areas, the stability equation was next used to determine the position of the center of pressure at flight Mach numbers. For each configuration, the stability equation (8) becomes:

Configuration A

$$292 + 35 \sqrt{M^2-1} \left(\frac{dC_L}{d\alpha}\right)_N = \left[42.2 + \sqrt{M^2-1} \left(\frac{dC_L}{d\alpha}\right)_N\right] l_{c.p.}$$

Configuration B

$$493 + 35 \sqrt{M^2-1} \left(\frac{dC_L}{d\alpha}\right)_N = \left[57.1 + \sqrt{M^2-1} \left(\frac{dC_L}{d\alpha}\right)_N\right] l_{c.p.}$$

Configuration C

$$692 + 35\sqrt{M^2-1}\left(\frac{dC_L}{d\alpha}\right)_N = \left[71.7+\sqrt{M^2-1}\left(\frac{dC_L}{d\alpha}\right)_N\right] \ell_{c.p.}$$

The solutions of these equations are shown in Fig. 5, where center of pressure and center of gravity positions are plotted for flight Mach numbers.

The problem of missile stability for wing angles of attack other than zero is simplified by the fact that the wing center of pressure is assumed to be located at the missile center of gravity. The added lift due to wing angle of attack will move the center of pressure forward from the position shown in Fig. 5. The center of pressure will not move forward of the center of gravity due to this added lift, however, since the lift is acting at the center of gravity. Accordingly, the missile will be stable or unstable as shown by Fig. 5. The stabilizing or destabilizing moment will be less than that shown by an amount dependent upon wing angle of attack.

IV. DRAG ANALYSIS

The drag for each of the rocket configurations was assumed to be made up of the following components:

Body Drag:
- a) Base
- b) Nose (Wave)
- c) Friction

Wing Drag:
- a) Friction
- b) Wave
- c) - Induced

Tail Drag:
- a) Friction
- b) Wave

Each of the drag components was evaluated in the supersonic case as follows:

I. Body Drag:

The base drag was obtained from the base pressure coefficient, $\frac{P_B}{q}$, defined by

$$\text{Base drag} = \left(\frac{P_B}{q}\right) q \frac{\pi d^2}{4}$$

This coefficient was considered from the viewpoint of Refs. 8, 9, and 10. A comparison of values obtained by each method is shown in Fig. 8. Values directly from Ref. 9 were used in the range of Mach numbers from 1.25 to 4.0. For higher Mach numbers, this curve of the base drag coefficient versus Mach number was extrapolated as shown in Fig. 8.

The values of wave drag coefficient were obtained from Ref. 11, in which tabulated values are given as functions of Mach number and cone half angle, θ_S. The cone half angle for this rocket

configuration is 7.1 degrees and interpolation in the tables between cone half angles of 5 degrees and 7.5 degrees established the values of wave drag coefficient as plotted in Fig. 9.

Skin friction drag was obtained by use of a constant skin friction coefficient of .002 based on total surface area. Therefore,

$$\text{Friction drag} = .002\, S_{\text{surface}} \times q$$

II. Wing and Tail Drag:

Skin friction drag was evaluated by use of a skin friction coefficient of .002.

Wave drag and induced drag were obtained from Ref. 12 which gives the following formula for the total drag (without friction) for thin circular arc airfoils at angles of attack:

$$C_{Dw} = \frac{4\alpha^2}{m} + \frac{16}{3m}\left(\frac{t_w}{c}\right)^2$$

where,

$$m = \sqrt{M^2-1}$$

Applying this formula to a 6 percent thick airfoil

$$C_{Dw} = \frac{.0192}{\sqrt{M^2-1}} + \frac{.00122\alpha^2}{\sqrt{M^2-1}}$$

for α in degrees. This formula for wing drag is based on wing area. It applies to wing and tail surfaces. Fig. 10 shows the total drag coefficient for the wing and tail surfaces.

In the subsonic region, induced drag was assumed zero since the proposed trajectory called for zero wing deflection during the initial verti-

cal flight. The wave drag coefficient was assumed to be replaced by a form drag coefficient which was arbitrarily set at .001 based on wing projected area. Base drag was estimated from results available on the German A-4 and A-9 missiles (Cf. Ref. 13).

The total drag coefficient for the rocket at various wing angles of attack and various Mach numbers was obtained from the following equation:

$$C_D = C_{D_{OB}} + C_{D_{OT}} + C_{D_{OW}} + C_{D_{iW}}$$

where each of the components were obtained as follows:

$$C_{D_{OB}} = C_{D_f} + C_{D_N} + \frac{P_B}{q}$$

$$C_{D_{OT}} = C_{D_f} + \frac{16}{3m}\left(\frac{t_w}{c}\right)^2$$

$$C_{D_{OW}} = C_{D_f} + \text{"}$$

$$C_{D_{iW}} = \frac{.0122\alpha_w^2}{\sqrt{M^2-1}}$$

These values of drag coefficient were converted to a reference area equal to the square of the body diameter and were plotted in Figs. 11, 12, 13, and 14.

This drag analysis does not consider the following factors:

a) Body-wing interference effects

b) Wing-tail interference effects

c) Change of base drag for jet burning (Cf. Ref. 13)

d) Change of skin friction drag with Reynolds number

Since drag effects are comparatively unimportant for rockets with high values of μ (Cf. Ref. 1), the assumptions made in this analysis will have less effect on rocket performance than any of the other approximations mentioned in the introduction.

V. ANALYSIS OF LIFT AND LIFT-DRAG RATIO

It has been assumed that the rocket remains at zero angle of attack throughout the flight and that the wing is rotated to give lift during the inclined portion of the trajectory. Since the rocket is at supersonic speeds throughout the inclined trajectory, analysis of the lifting force of the wing is necessary only for supersonic speeds.

The lift coefficient, C_{Lw}, for the wing is determined from :

$$C_{Lw} = \frac{.070 \alpha_w}{\sqrt{M^2-1}}$$

where α_w is measured in degrees and the lift force is based on wing projected area. The curves of wing lift coefficient versus Mach number of Fig. 15 were obtained from this equation.

The lift-drag ratio of each configuration is of interest since this ratio determined the angle of glide for the glide path portion of the trajectory. Values of the lift-drag ratio as function of Mach number and wing angle of attack are useful in the trajectory calculations.

The angles of attack for maximum lift-drag ratio for each configuration were obtained by minimizing the equations for the ratio of drag coefficient to lift coefficient as follows:

$$C_D = C_{D_{OB}} + C_{D_{OT}} + C_{D_{OW}} + C_{D_{iW}}$$

$$= C_{D_O} + C_{D_{iW}}$$

$$C_D = C_{D_O} + \frac{.0122 \alpha_w^2}{\sqrt{M^2-1}}$$

$$\alpha_w^2 = \left[C_{Lw} \Big/ \left(\frac{dC_L}{d\alpha}\right)_w \right]^2 = C_{Lw}^2 \quad \frac{M2-1}{16}$$

Substituting

$$C_D = .00305\sqrt{M^2-1}\ C_{L_W}^2 + C_{D_O}$$

$$\frac{C_D}{C_{L_W}} = .00305\sqrt{M^2-1}\ C_{L_W} + \frac{C_{D_O}}{C_{L_W}}$$

Differentiating

$$\frac{\partial}{\partial C_{L_W}}\left(\frac{C_D}{C_{L_W}}\right) = .00305\sqrt{M^2-1} - \frac{C_{D_O}}{C_{L_W}^2}$$

For minimum $\frac{C_D}{C_{L_W}}$:

$$C_{D_O} = .00305\sqrt{M^2-1}\ C_{L_W}^2$$

or $$C_{D_O} = C_{D_{iW}}$$

The curves of wing angle of attack for maximum lift-drag ratio (Cf. Fig. 16) were obtained by graphically solving the equation for total parasite drag equal to wing induced drag at flight Mach number. Values of the lift-drag ratio versus Mach number are shown in Figs. 18, 19, and 20. Maximum lift-drag ratios are shown in Fig. 17.

VI. THRUST VARIATION WITH ALTITUDE

For each of the three thrust programs under consideration, an approximation to the change of thrust with altitude must be made. Selection of sea level values for specific impulse and burning rate specify the values of thrust at sea level, since

$$F_{\text{sea level}} = I_{sp}\,\dot{W}_p$$

The decrease of atmospheric pressure with altitude, however, causes an increase in thrust over the sea level values. The magnitude of this increase is dependent upon nozzle configuration.

The variation of thrust with altitude may be computed from the following formula

$$F = \text{velocity thrust} + \text{pressure thrust}$$
$$= F_V + (P_e - P_0) f_e$$

The values of velocity thrust are determined from specified sea level values of total thrust and atmospheric pressure and from design values of exit pressure and exit area. Nozzle design determines P_e and f_e and thus, the value of pressure thrust at altitude.

It may be shown (Cf. Ref. 1) that maximum thrust at any altitude is obtained when the nozzle throat area to exit area ratio, ϵ , is established to give optimum expansion, i.e., zero pressure thrust since P_e and P_0 are equal for optimum expansion. Therefore, selection of a single design nozzle configuration gives maximum thrust at one altitude only. If this design configuration is selected to give maximum thrust near the midpoint of propellant burning time, the thrust decrement for higher and lower altitudes will not be great.

Further design conditions on nozzle shape are the rocket motor chamber pressure determined by

$$P_c = \frac{F}{C_F f_t}$$

and the missile outside diameter which limits the maximum size of the nozzle exit area. Selection of an exit area, f_e, of 700 in.^{2} and a throat area, f_t, of 70 in.^{2} gives rocket motor characteristics as shown in Table II.

Thrust variations with altitude as shown in Fig. 21 were obtained from the following equations

Case I:

$$F = 58{,}000 + (6.3 - P_o)\ 700$$

Case II:

$$F = 41{,}500 + (4.2 - P_o)\ 700$$

Case III:

$$F = 26{,}800 + (1.7 - P_o)\ 700$$

VII. EQUATIONS OF MOTION AND TRAJECTORY CALCULATION PROCEDURE

The following equations of motion were utilized in the trajectory analyses (Cf. Ref. 4):

Along the flight path

$$\frac{W}{g}\frac{dV}{dt} = F - D - W \sin\theta$$

Normal to the flight path

$$V\frac{d\theta}{dt} = -g\cos\theta + \frac{L}{W}g$$

On fixed coordinates

$$\frac{dx}{dt} = V\cos\theta$$

$$\frac{dy}{dt} = V\sin\theta$$

These equations are general and were applied to the boost, powered and glide phases of the trajectory.

The rocket trajectories were computed by a step-by-step integration of the equations of motion. The following relations were used to determine quantities appearing in these equations:

$$W = W_0 - \dot{W}_p\frac{t}{t_p}$$

$$D = C_D\frac{\sigma\rho_0}{2}V^2d^2$$

$$L = C_L\frac{\sigma\rho_0}{2}V^2d^2$$

where C_D and C_L are found for the Mach numbers and wing angles of attack.

Two types of corrections must be applied to rockets which reach very high altitudes or long ranges. The first is due to the variation of gravity with altitude. This correction is given by

$$g_y = g\left(\frac{R}{R+y}\right)^2$$

where g_y is the acceleration due to gravity at the altitude y. The second correction is due to the difference between the horizontal range and the range measured along the surface of the earth. This correction is also a function of the altitude of the trajectory (Cf. Ref. 15). Since the trajectories being investigated have summit altitudes of less than 1,000,000 feet these corrections are of small magnitude and are omitted in the step-by-step integrations.

VIII. DISCUSSION OF RESULTS

Four vertical trajectories were computed by the step-by-step integration method. The results, i.e., altitude and velocity, are shown plotted against time in Figs. 22 and 23. Configuration D achieves higher altitudes and velocities than configuration A because of the decreased drag and weight of the wingless rocket. Higher performance is achieved in Case III for either rocket; in Case III, the thrust phase is made up of a 10 second boost and 78 second cruise period. Increases of the summit altitude, y_s, of approximately 9 percent resulted for each configuration with the two stage thrust period.

The increase in altitude resulting from the two stage thrust period is a net effect of three factors. The primary cause is an increase in total impulse; the total impulse, i.e., integral of the thrust time curve, is approximately 15 percent higher for Case III than for Case I. Secondary factors are the drag decrease and inertial force increase for the two stage case. Drag forces are decreased slightly because the rocket has smaller velocities in the low altitude portion of the trajectory. Inertial forces are increased by the slower burning rate of the propellant. Since the altitude is not increased proportionately with the increase in total impulse, it is evident that the decrement due to increase of inertial force is of greater magnitude than the increment due to decrease of drag force.

The maximum range of a vacuum trajectory is approximately twice the summit altitude of a vertical trajectory (Cf. Ref. 4). Accordingly, approximations to the maximum ballistic ranges for the configurations would be as follows:

Configuration A:		
Case I	1,600,000 ft.	(300 mi.)
Case III	1,760,000 ft.	(334 mi.)
Configuration D		
Case I	1,744,000 ft.	(330 mi.)
Case III	1,910,000 ft.	(360 mi.)

One horizontal trajectory was computed for Configuration A with the constant thrust program designated Case I. The altitude, velocity and horizontal range for this trajectory are shown in Fig. 24. The range at impact is 1,384,000 ft. or approximately 262 miles. The maximum velocity reached is 6360 feet per second at the end of burning of the propellant. This velocity corresponds to a Mach number of 6.5.

This horizontal trajectory is of interest because it indicates the general nature of the powered, ballistic and glide path trajectory of the winged rocket of Configuration A. To obtain the maximum horizontal range, various values of the flight path angle, θ , must be used.

The effect on horizontal range of adding a wing to a rocket could be obtained by comparison of the maximum ranges of Configurations A and D as computed by step-by-step integration methods. The effect of wing area could be evaluated similarly by comparison of the performance of Configurations A, B and C.

APPENDIX I

SUMMARY OF GERMAN A-9 PROJECT

General

The German A-9 missile was a winged version of the A-4 long-distance rocket (Cf. Ref. 13). Development was not completed due to the end of the war, but considerable data was collected on the aerodynamic characteristics of various wing plus tail configurations and on the theoretical performance of the A-9 as a single stage missile or as the glider stage of a two-stage missile. As a further development it was intended to convert the A-9 into a crew carrying missile with manual steering, retractable landing gear and special aerodynamic aids to reduce the landing speed to approximately 160 kilometers per hour. This crew-carrying version was to go 600 kilometers in approximately 17 minutes.

The single stage A-9 missile was developed in an effort to increase the range of the A-4 from 270 kilometers to 450 kilometers. Sixteen wing and tail configurations on the standard A-4 fuselage were tested in subsonic and supersonic wind tunnels, and aerodynamic studies were continuing at the end of the war. Several trajectories were computed in an effort to ascertain the maximum range possible based on assumed aerodynamic properties.

The two-stage version of the A-9 was considered because the range of either the piloted or pilotless versions could be increased considerably if the A-9 propulsion unit could be started after the rocket had reached a certain initial velocity. The first stage, a large assisted-take-off rocket designated the A-10, was designed to give the A-9 an initial velocity of 1200 meters per second.

The A-9 separated at the end of the burning period of the A-10 booster, and continued in a combined power and glide path trajectory. Under these circumstances, the A-9 would have a range of approximately 5000 kilometers. The proposed design of the A-10 booster stage specified development of 200 tons thrust and installation of air brakes and a parachute to permit reuse after water impact.

Development of the Single Stage Version

The first step in the development of the A-9 missile was the determination, from wind tunnel test results, of the lift-drag ratio and the center of pressure movement for each of sixteen wing plus tail configurations at subsonic and supersonic velocities and for an angle of attack range of 0 to 8 degrees. The configuration finally selected was the A4V12/c shown in Fig. 1. This model had the highest lift-drag ratio of all models tested, but also had excessive shift of the center of pressure in the transonic speed range.

After selection of the basic configuration, studies were continued in an effort to reduce movement of the center of pressure during transition from subsonic to supersonic speeds. Data on effects of span of swept wings, wing position and airfoil section were being obtained at the end of the war.

Several trajectories were computed for the single stage version. In the first, the missile was launched vertically to propellant cut-off and continued to a maximum height of 80 kilometers. At this height, the air density was too low to support gliding of the A4V12/c and the missile fell in a ballistic trajectory and oscillated after entry into the lower

atmosphere. Load factors and control requirements were excessive for this trajectory. A flat-path trajectory with a summit altitude of approximately 40 kilometers was calculated to give the maximum range of 450 kilometers for the A4V12/c.

Development of the Two-Stage Version

Work on the two—stage version of the A-9 was limited to basic design and trajectory studies based on aerodynamic data being collected on the glider A4V12/c. Basic assumptions for the trajectory studies were as follows:

First Stage: A 10 Booster Rocket

Combustion time: 60 seconds

Weight:	Payload	16,260 Kg
	Frame	17,000
	Fuel	48,156

Caliber: 4.15 meters

Second Stage: A-9 (Glider A4V12/c)

Combustion time: 103.8 seconds

Weight:	Payload	1,000 Kg
	Frame	3,000
	Fuel	11,575

Caliber: 1.65 meters

Four investigations were made in an effort to determine which trajectory would give the longest range with permissible wing loadings. The first two investigations assumed the second stage combustion to follow

immediately after the first and that the missile would traverse a skip trajectory after reentering the lower atmosphere. As a result of the first two analyses, it was determined that the whole trajectory should be made at the lower levels of the atmosphere. The third investigation assumed, therefore, that the second combustion stage would begin after the vertex was reached and that the thrust would be utilized for the pull-out and for orienting the missile for gliding. The fourth investigation delayed the second-stage combustion for 16 seconds after the end of burning of the booster stage. The glider was then turned uniformly 90 degrees during the second combustion period in order to have it at the proper stage.

REFERENCES

1) Seifert, H. S., Mills, M. M., Summerfield, M., "The Physics of Rockets", Reprint, American Journal of Physics, Vol. 15 (1947).

2) Diehl, Walter S. "Standard Atmosphere - Tables and Data", NACA Report 218 (1925).

3) Warfield, Calvin N., "Tentative Tables for the Properties of the Upper Atmosphere", NACA Technical Note 1200 (1947).

4) Stewart, H. J., Lecture Notes, Course in Jet Propulsion Systems, California Institute of Technology (1949).

5) Walther, A., and Thiel, A., "Report on Glider Missile", Peenemunde Report, Archive 50/8 gK (1942).

6) Spreiter, John R., "Aerodynamic Properties of Slender Wing Body Combinations at Subsonic, Transonic and Supersonic Speeds", NACA Technical Note 1662 (1948).

7) Puckett, A.E., and Stewart, H. J., "Aerodynamic Performance of Delta Wings at Supersonic Speeds", Journal of Aeronautical Sciences, Vol. 14 (1947).

8) von Karman, Th., and Moore, N. B., "Resistance of Slender Bodies Moving with Supersonic Velocities with Special Reference to Projectiles", ASME Transactions (1932).

9) Hill, F. K., and Alpher, R. A., "Base Pressures at Supersonic Velocities", Journal of Aeronautical Sciences, Vol. 16 (1949).

10) Charters, A. C., "Some Ballistic Contributions to Aerodynamics", Journal of Aeronautical Sciences, Vol. 14 (1947).

11) Kopal, Zdenek, "Tables of Supersonic Flow Around Cones", Massachusetts Institute of Technology Technical Report No. 1 (1947).

12) Liepmann, H. W., and Puckett, A. E., "Aerodynamics of a Compressible Fluid", Wiley (1947).

13) Zwicky, F., "Report on Certain Phases of War Research in Germany, AMC Report F-SU-3-RE-(1947).

14) Hayes, T. J., "Elements of Ordnance", Wiley (1938).

15) Kooy, J. M. J., and Uytenbogaart, J. W. H., "Ballistics of the Future", McGraw Hill (1946).

TABLE I

DESIGN CHARACTERISTICS OF ROCKET CONFIGURATIONS

Characteristic	Config. A	Config. B	Config. C	Config. D
Body length (ft.)	35	35	35	35
Body diameter (ft.)	2.5	2.5	2.5	2.5
Length/diameter	14	14	14	14
Nose cone length (ft.)	10	10	10	10
Nose cone half angle	7.1°	7.1°	7.1°	7.1°
Tail area (ft.)	92	98.6	104.4	85
Tail span (ft.)	4.3	4.5	4.6	4.2
Tail root chord (ft.)	6.5	6.7	6.9	6.3
Wing area ($ft.^2$)	20	40	60	--
Wing span (ft.)	3.3	4	4.6	--
Wing root chord (ft.)	5	7	9.2	--
Maximum angle of attack of wing	14°	12°	10°	--
Sweep back of tail & wing L.E.	60°	60°	60°	60°
Wing & tail percent thickness	6	6	6	6
Payload weight (lb.)	500	500	500	500
Structure Weight (lb.)	4000	4200	4400	3800
Propellant weight (lb.)	10,500	10,500	10,500	10,500
Gross weight (lb.)	15,000	15,200	15,400	14,800
Center of gravity location (ft. from base)	14.7	14.7	14.7	14.7
Propellant-gross weight ratio	0.7	0.69	0.68	0.71
Ratio of gross weight to cross sectional area ($lb./ft.^2$)	3040	3080	3130	3000

TABLE II

ROCKET POWER PLANT CHARACTERISTICS

Characteristic	Case I	Case II	Case III
Specific impulse at sea level (sec.)	200	190	180
Burning rate (lbs./sec.)	262.5	180	100
Burning time (sec.)	40	43.7	78.7
Sea level thrust (lbs.)	52,000	34,000	18,000
Chamber pressure (psi)	570	375	200
Nozzle throat area ($in.^2$)	70	70	70
Nozzle exit area ($in.^2$)	700	700	700
Expansion ratio,	10	10	10
Altitude for optimum expansion (ft.)	22,000	32,000	45,000

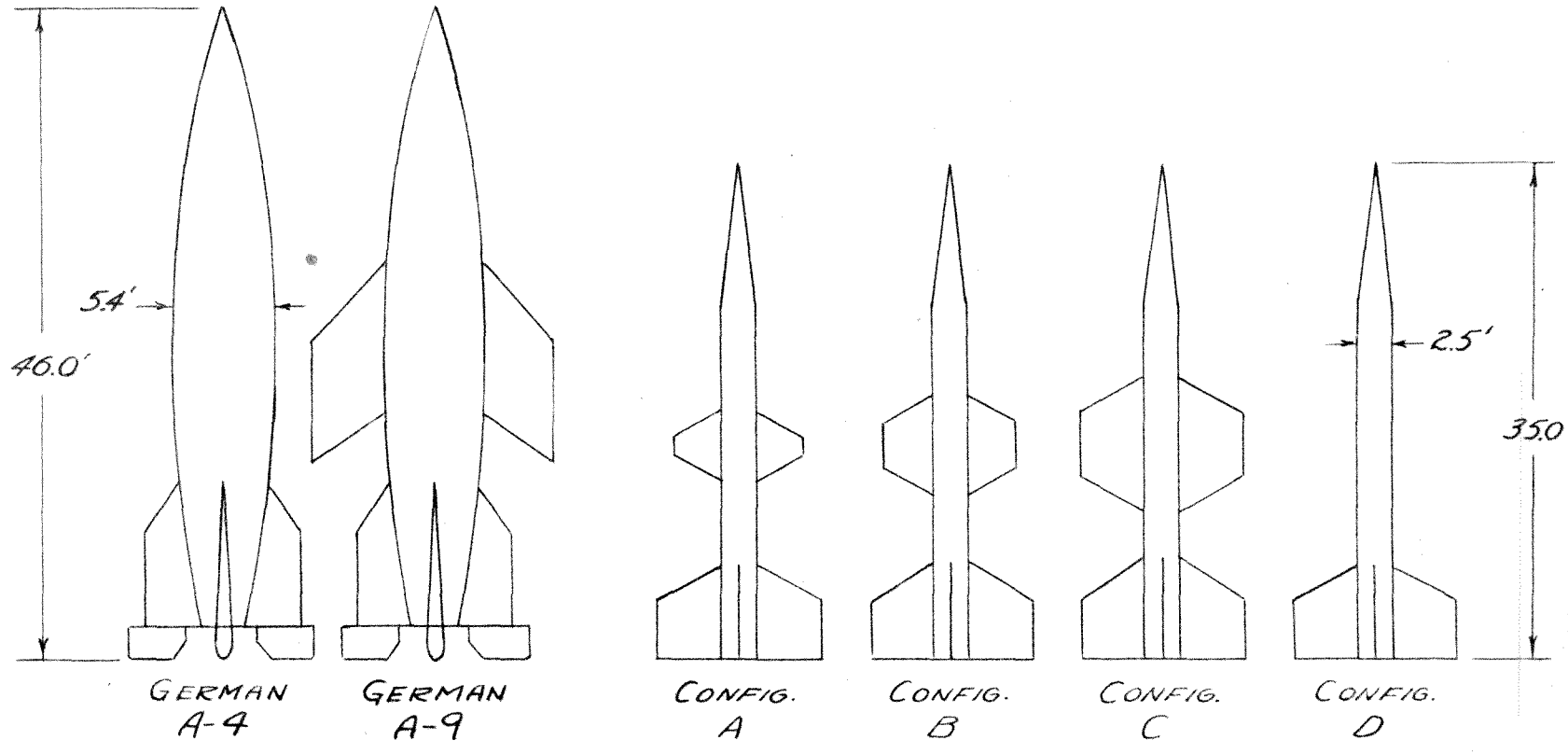

GROSS WEIGHT	30,000	35,200	15,000	15,200	15,400	14,800
PROP. WEIGHT	21,500	26,500	10,500	10,500	10,500	10,500
WING AREA		145	20	40	60	
TAIL AREA	75	75	92	98.6	104.4	85

FIGURE 1
ROCKET CONFIGURATIONS

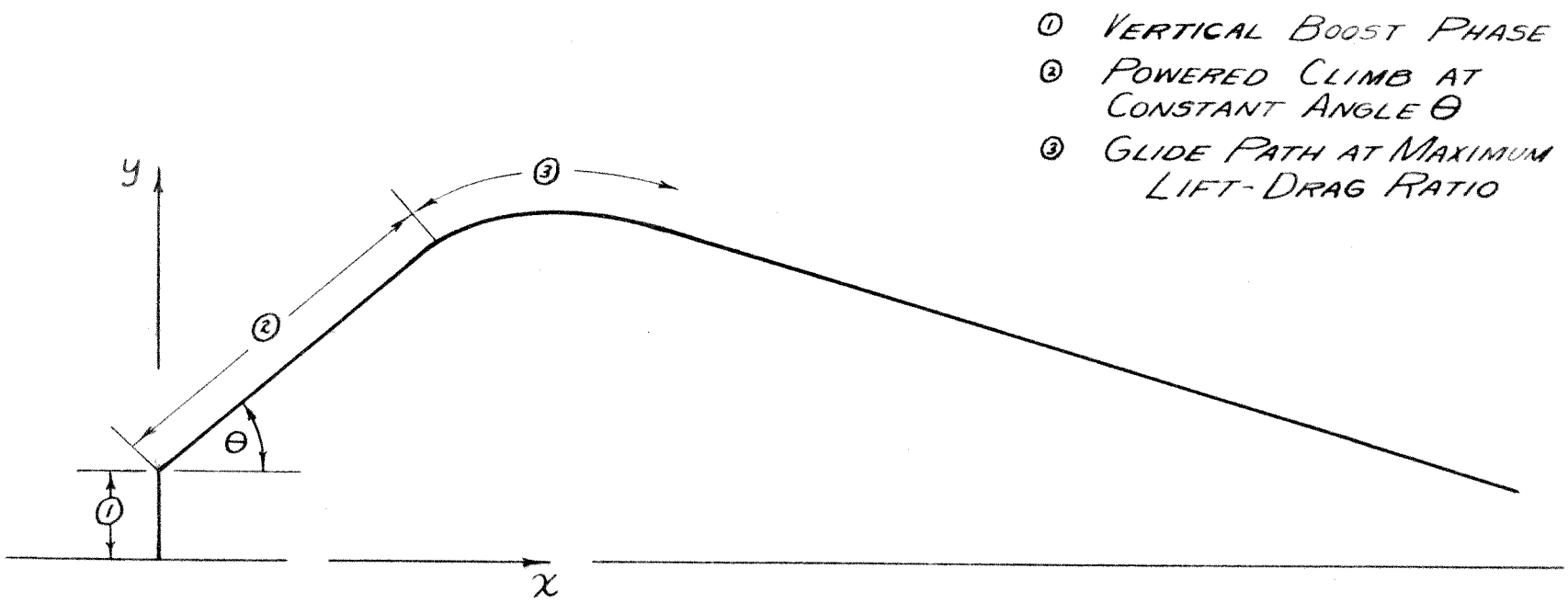

FIGURE 2
ROCKET TRAJECTORY

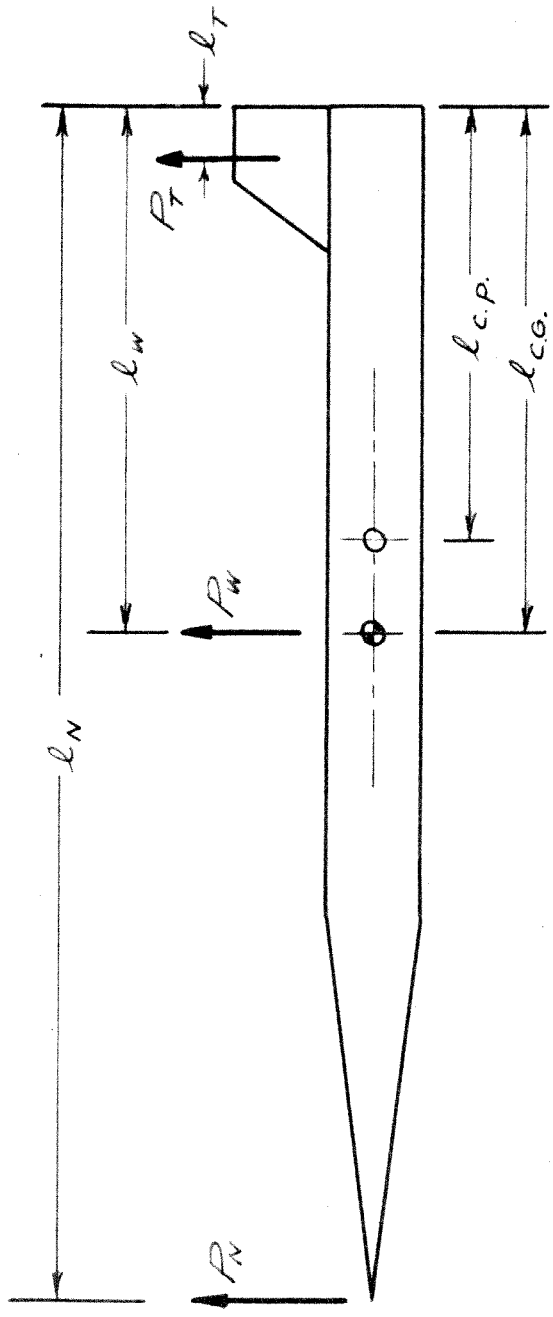

FIGURE 3
AERODYNAMIC FORCES ACTING ON ROCKET

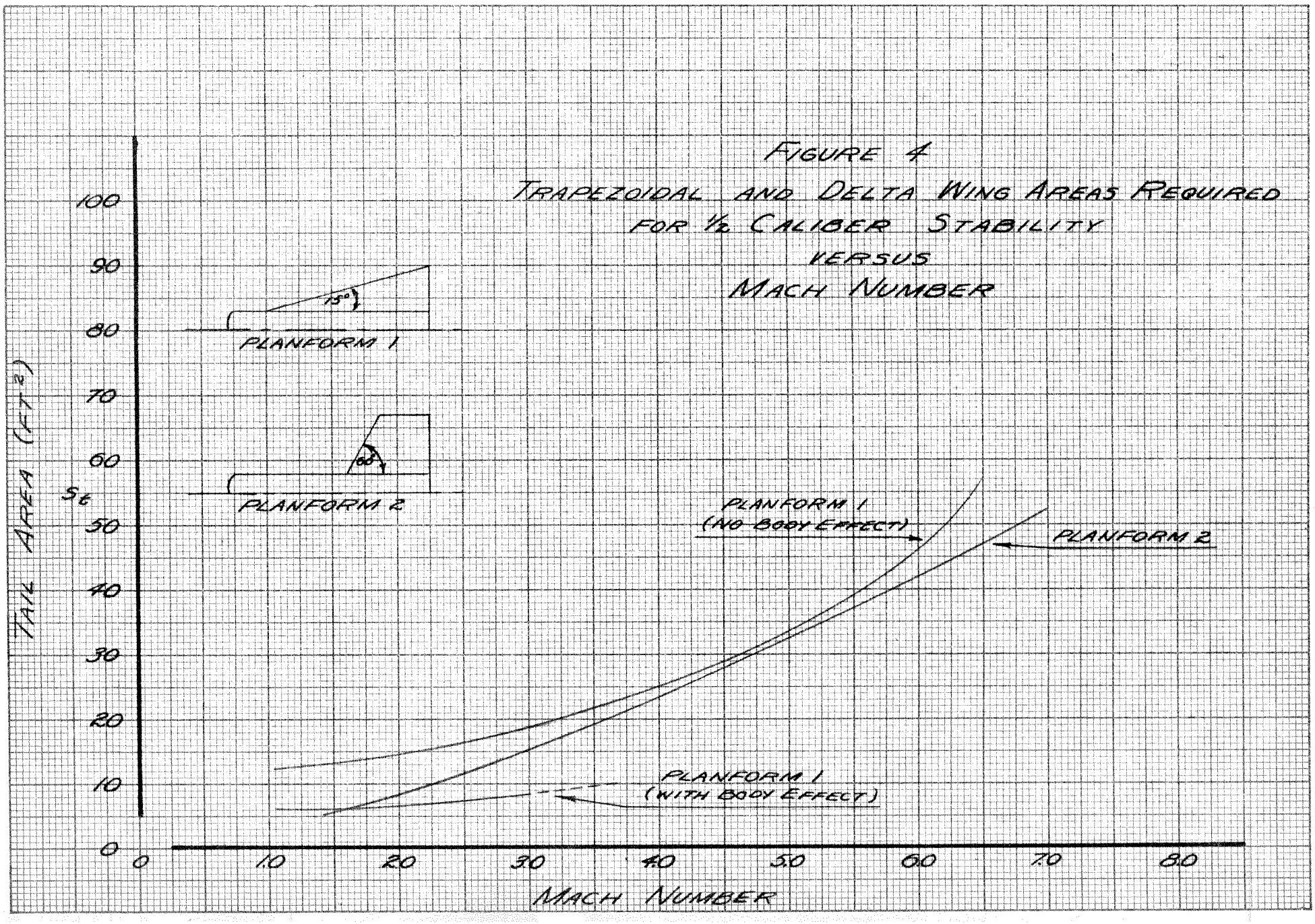
FIGURE 4
TRAPEZOIDAL AND DELTA WING AREAS REQUIRED FOR ½ CALIBER STABILITY VERSUS MACH NUMBER
TAIL AREA (FT²)
S_6
100
90
80
70
60
50
40
30
20
10
0
15°
PLANFORM 1
60°
PLANFORM 2
PLANFORM 1 (NO BODY EFFECT)
PLANFORM 2
PLANFORM 1 (WITH BODY EFFECT)
0
1.0
2.0
3.0
4.0
5.0
6.0
7.0
8.0
MACH NUMBER

FIGURE 5

CENTER OF PRESSURE MOVEMENT WITH MACH NUMBER

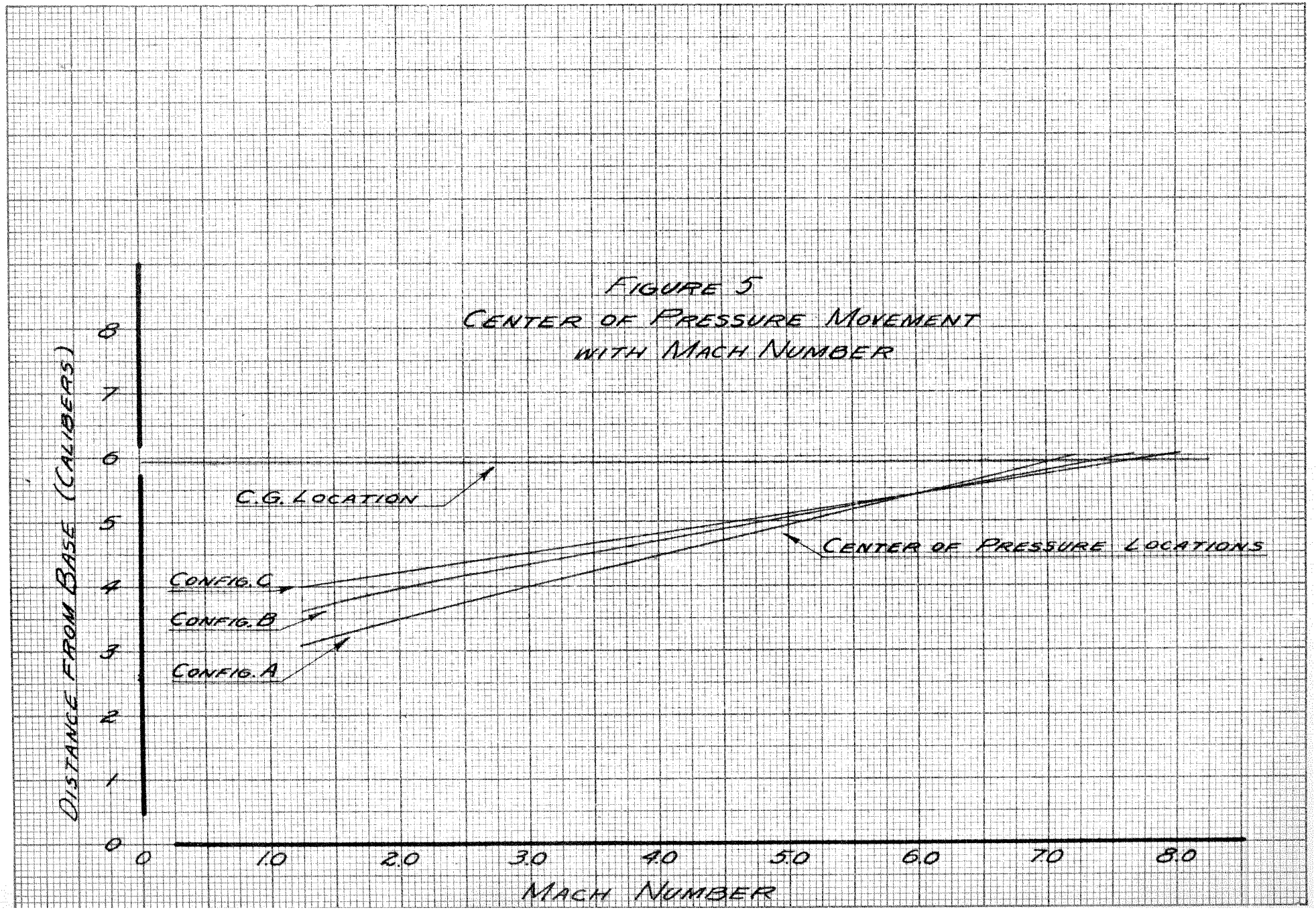

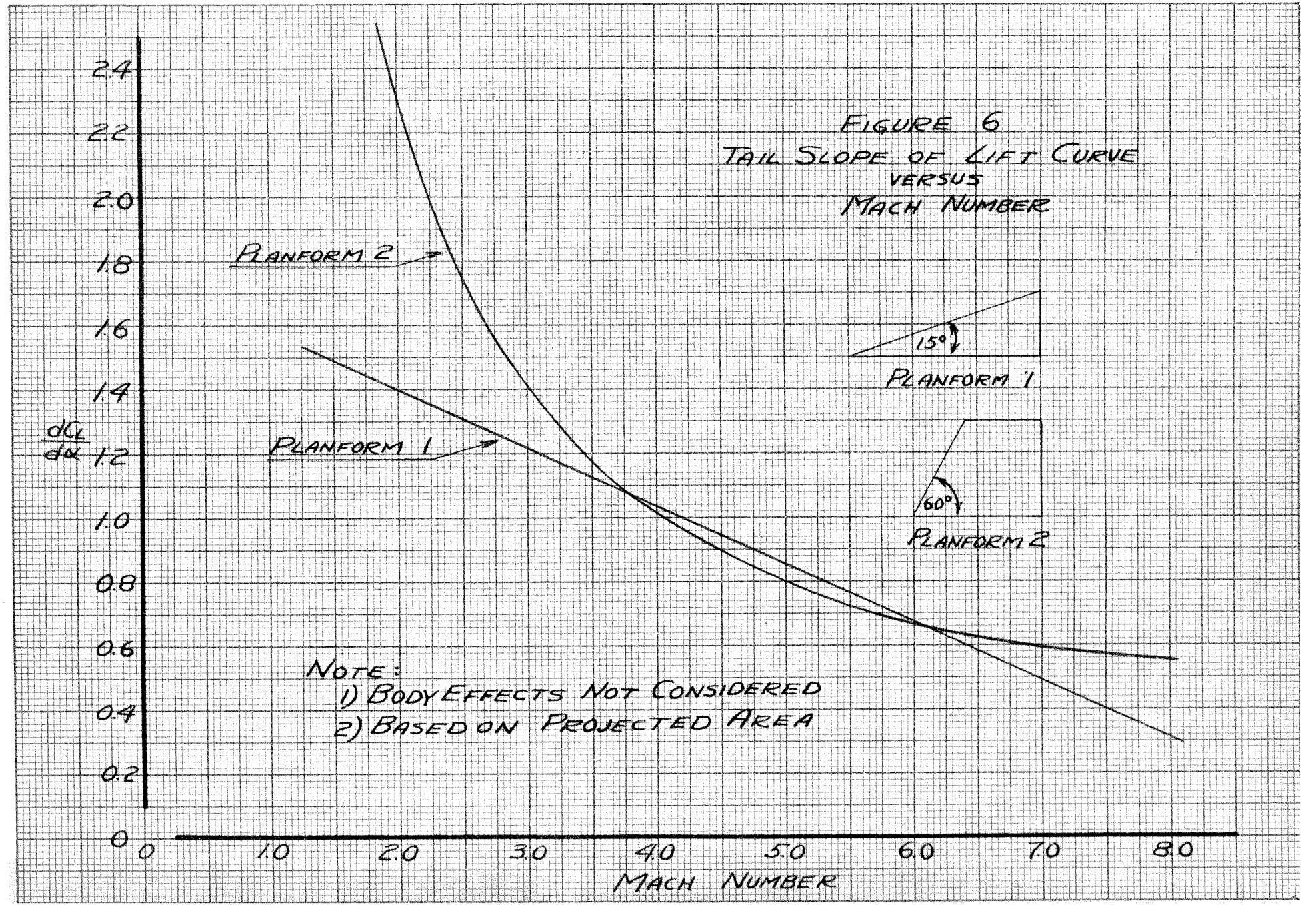
FIGURE 6
TAIL SLOPE OF LIFT CURVE
VERSUS
MACH NUMBER
PLANFORM 2
PLANFORM 1
15°
PLANFORM 1
60°
PLANFORM 2
NOTE:
1) BODY EFFECTS NOT CONSIDERED
2) BASED ON PROJECTED AREA
dCL/dα
2.4
2.2
2.0
1.8
1.6
1.4
1.2
1.0
0.8
0.6
0.4
0.2
0
0
1.0
2.0
3.0
4.0
5.0
6.0
7.0
8.0
MACH NUMBER

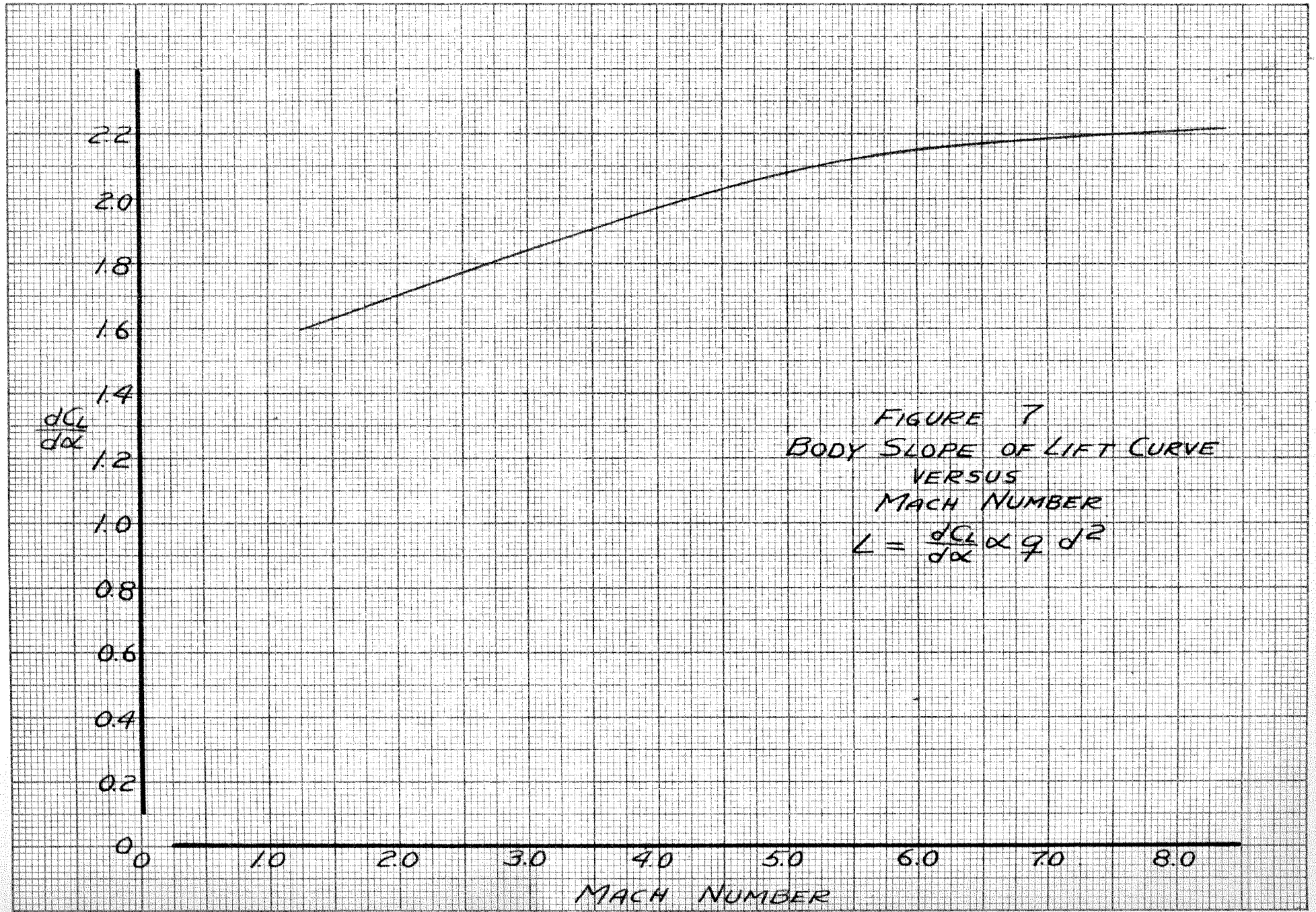

FIGURE 7
BODY SLOPE OF LIFT CURVE
VERSUS
MACH NUMBER

$$L = \frac{dC_L}{d\alpha} \alpha q d^2$$

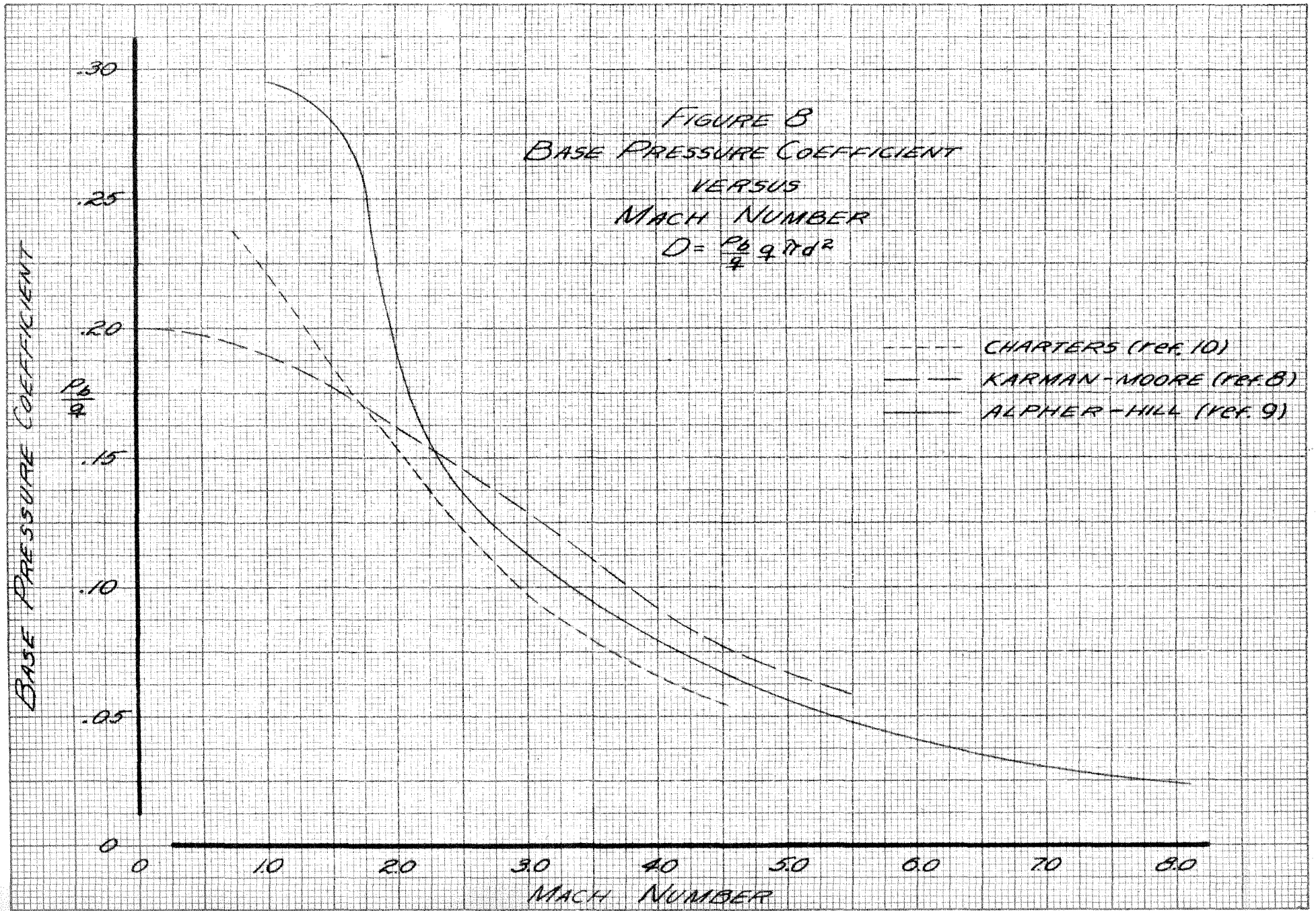
FIGURE 8
BASE PRESSURE COEFFICIENT
VERSUS
MACH NUMBER
$D = \frac{P_b}{q} q \pi d^2$
CHARTERS (REF. 10)
KARMAN-MOORE (REF. 8)
ALPHER-HILL (REF. 9)
BASE PRESSURE COEFFICIENT
$\frac{P_b}{q}$
.30
.25
.20
.15
.10
.05
0
0
1.0
2.0
3.0
4.0
5.0
6.0
7.0
8.0
MACH NUMBER

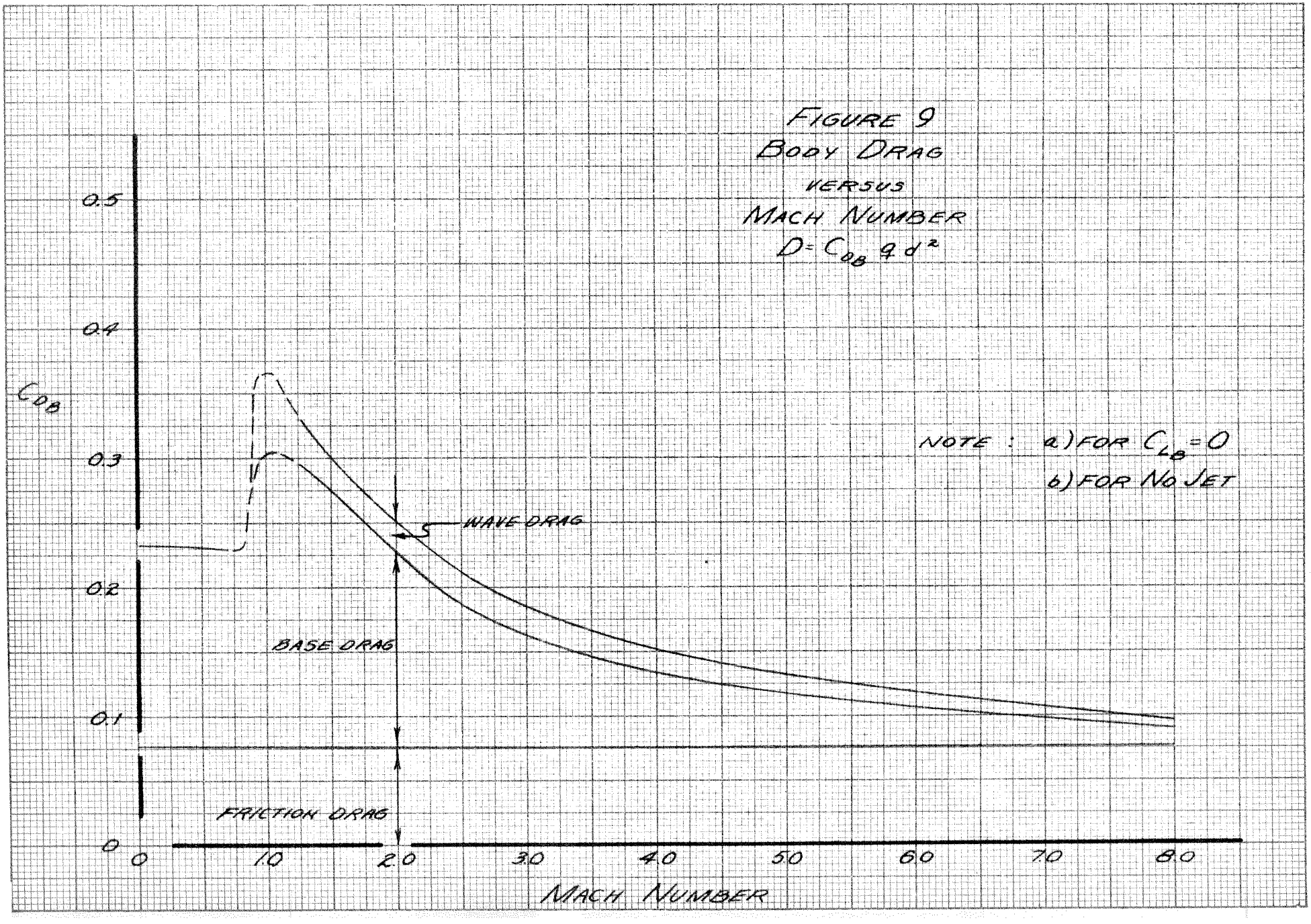
FIGURE 9
BODY DRAG
VERSUS
MACH NUMBER
$D = C_{DB}\, q\, d^2$
NOTE : a) FOR $C_{LB} = 0$
b) FOR NO JET
C_{DB}
0.5
0.4
0.3
0.2
0.1
0
WAVE DRAG
BASE DRAG
FRICTION DRAG
0
1.0
2.0
3.0
4.0
5.0
6.0
7.0
8.0
MACH NUMBER

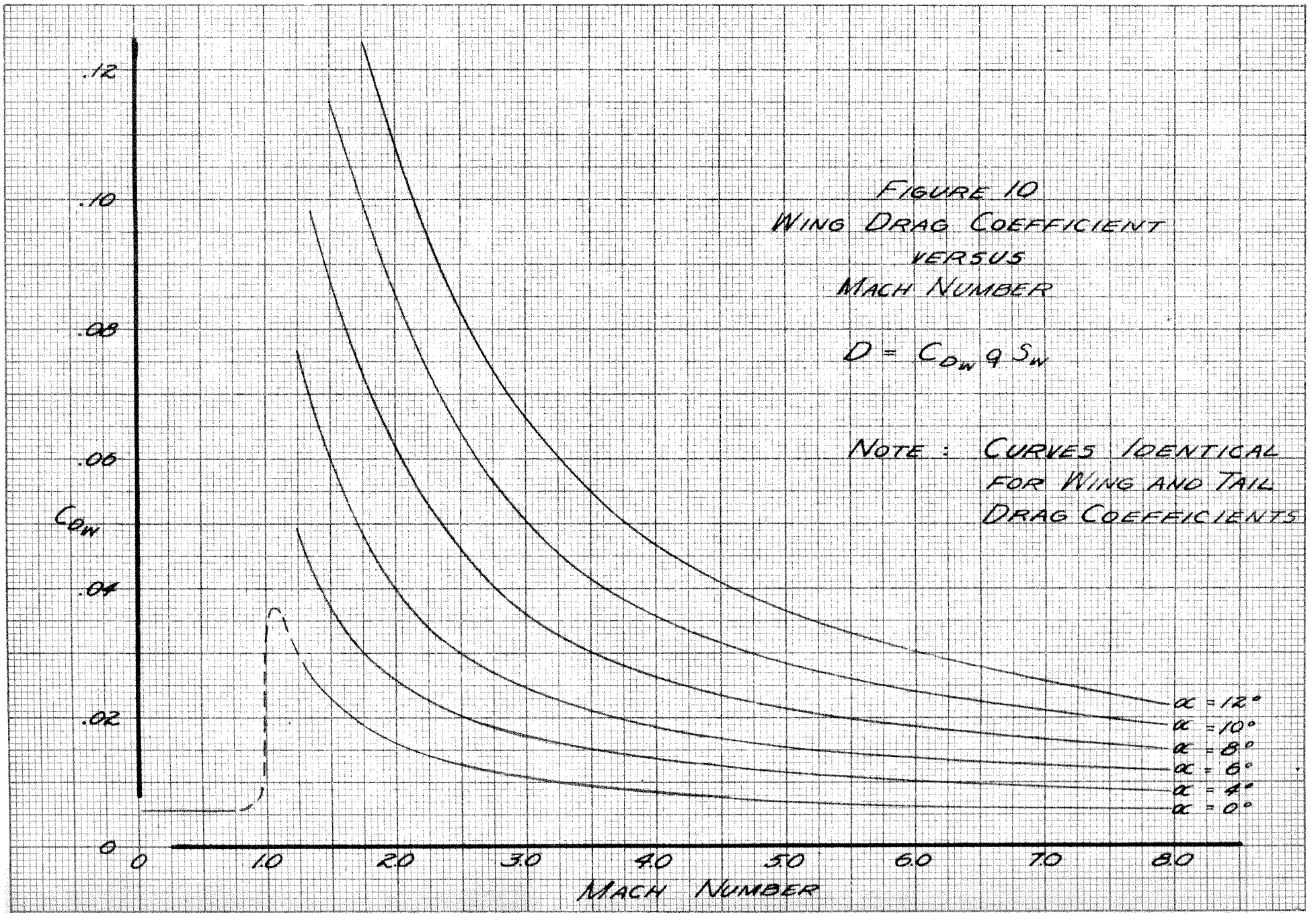

FIGURE 10
WING DRAG COEFFICIENT
VERSUS
MACH NUMBER

$D = C_{D_W} q S_W$

NOTE : CURVES IDENTICAL FOR WING AND TAIL DRAG COEFFICIENTS

FIGURE 11

DRAG COEFFICIENT VERSUS MACH NUMBER

CONFIGURATION A

DRAG = $C_D q d^2$

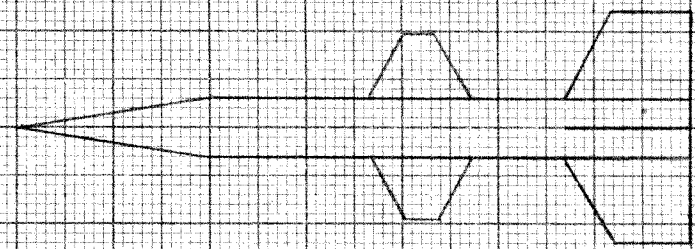

NOTE: TAILS ROTATED 45° FROM PLANE OF WING

FIGURE 12

DRAG COEFFICIENT VERSUS MACH NUMBER

CONFIGURATION B

DRAG = $C_D q d^2$

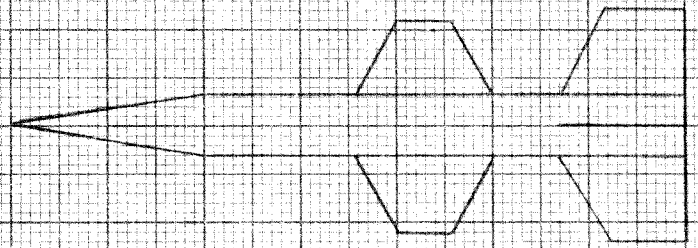

NOTE: TAILS ROTATED 45° FROM PLANE OF WING

DRAG COEFFICIENT C_D

1.0
0.9
0.8
0.7
0.6
0.5
0.4
0.3
0.2
0.1
0

0 1.0 2.0 3.0 4.0 5.0 6.0 7.0 8.0

MACH NUMBER

TOTAL DRAG

BODY DRAG

FIGURE 13

DRAG COEFFICIENT VERSUS MACH NUMBER

CONFIGURATION C

DRAG = $C_D q d^2$

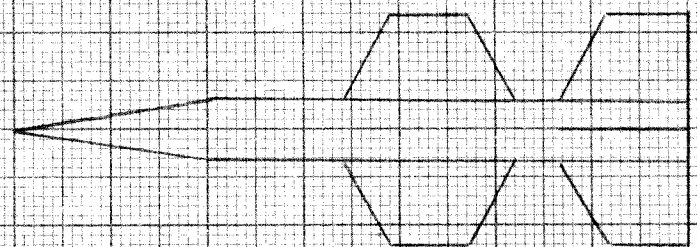

NOTE: TAILS ROTATED 45° FROM PLANE OF WING

FIGURE 14

DRAG COEFFICIENT VS. MACH NUMBER

CONFIGURATION D

DRAG = $C_D q d^2$

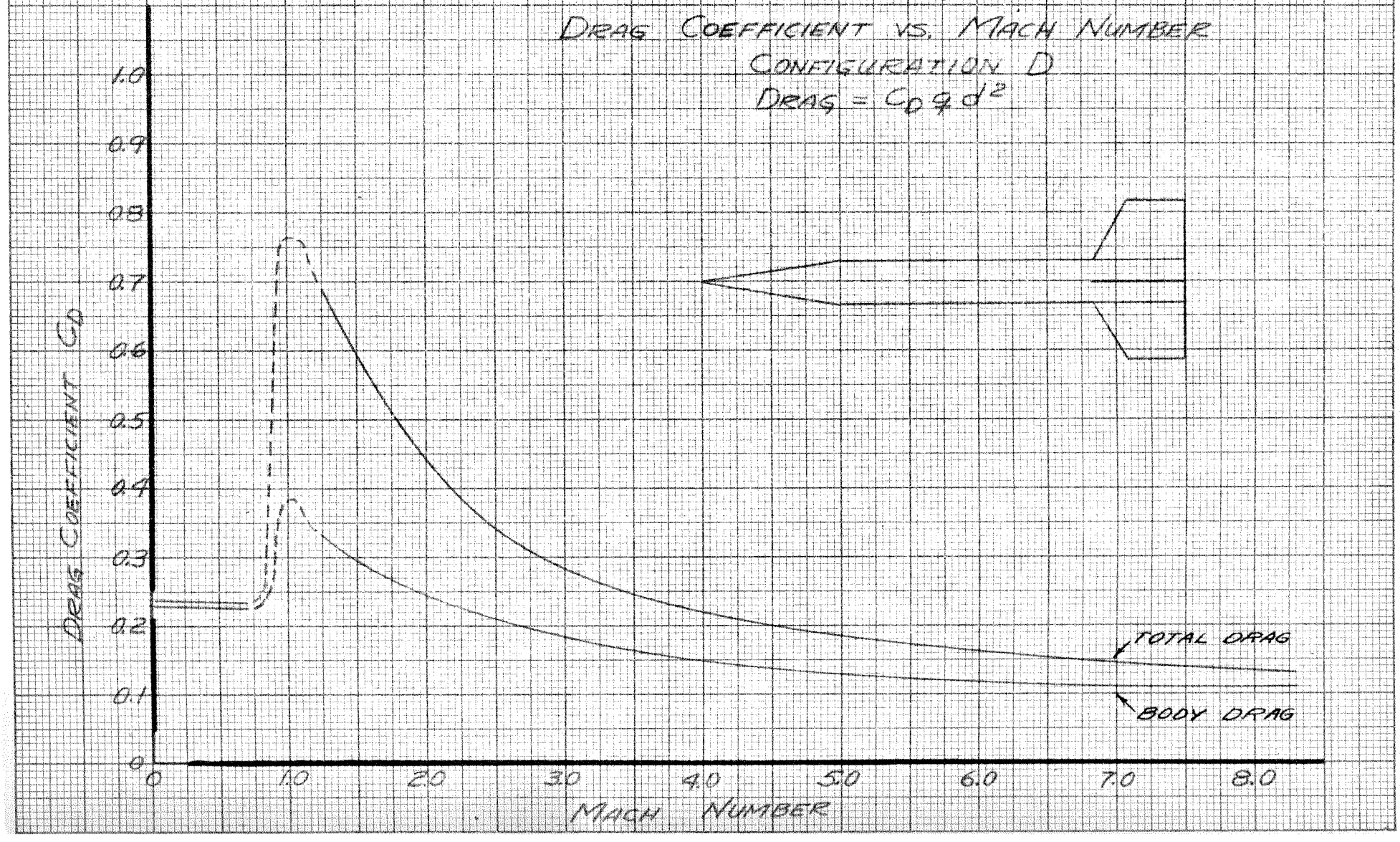

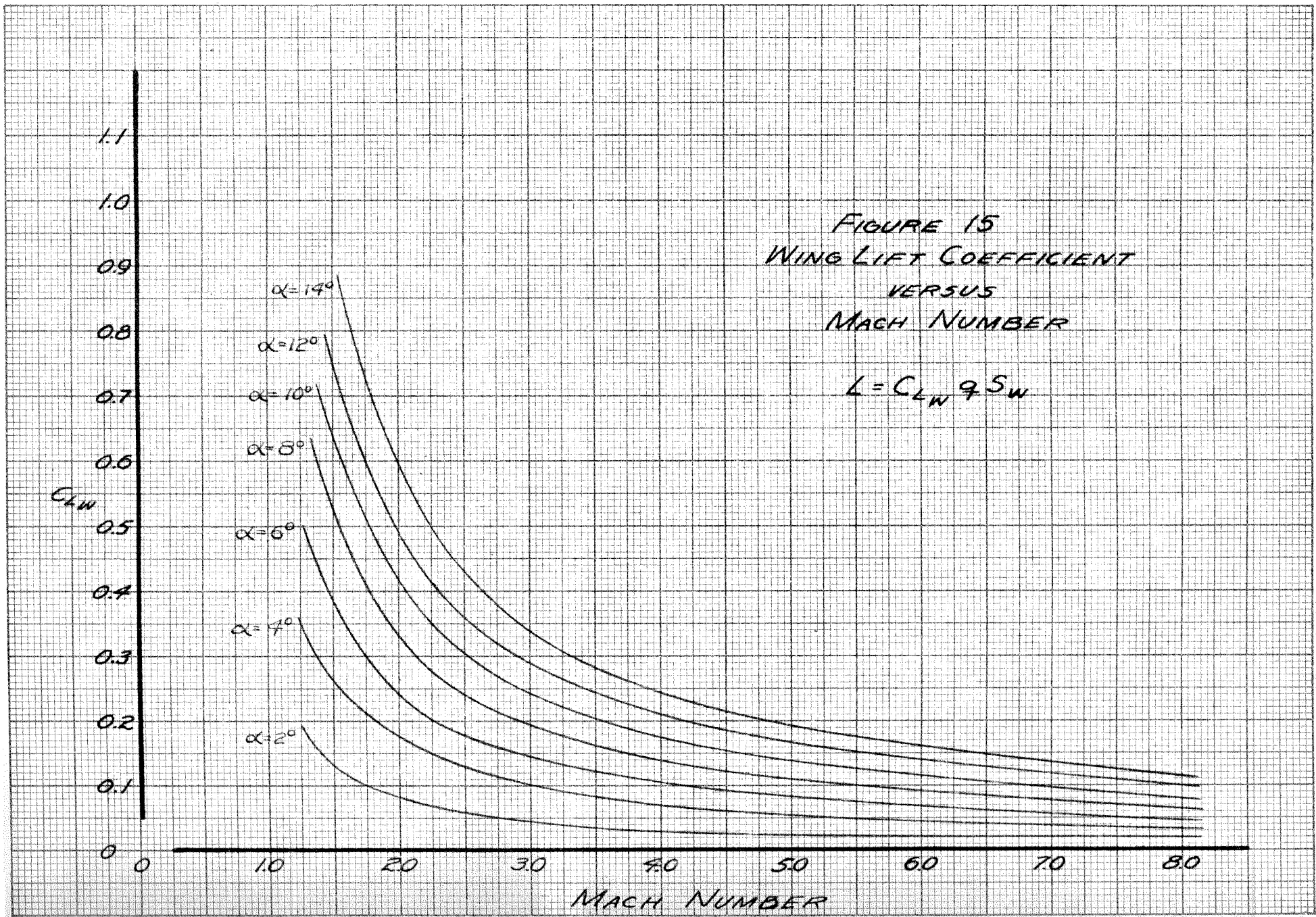

FIGURE 15
WING LIFT COEFFICIENT
VERSUS
MACH NUMBER

$L = C_{L_W} q S_W$

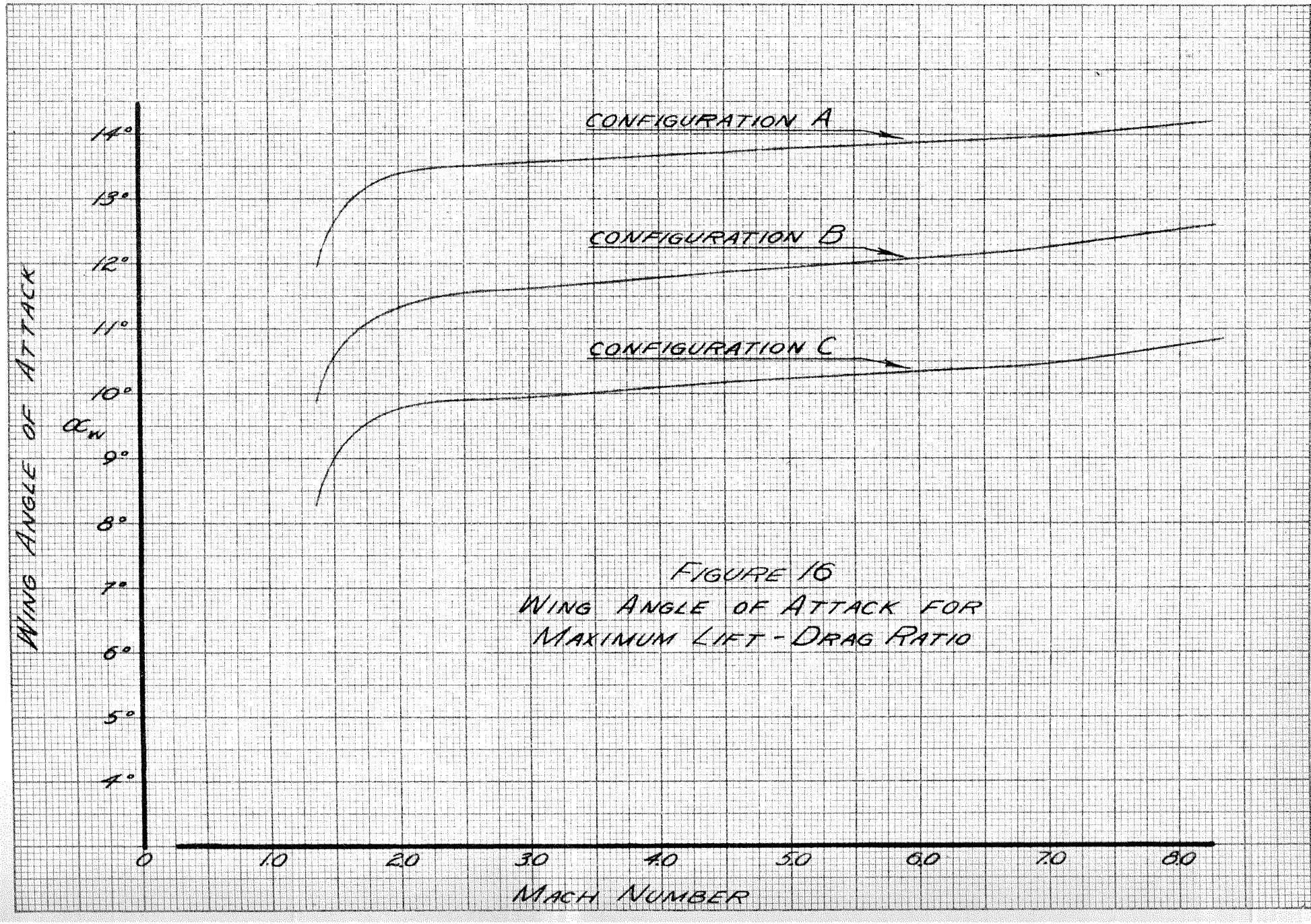

FIGURE 16
WING ANGLE OF ATTACK FOR
MAXIMUM LIFT - DRAG RATIO

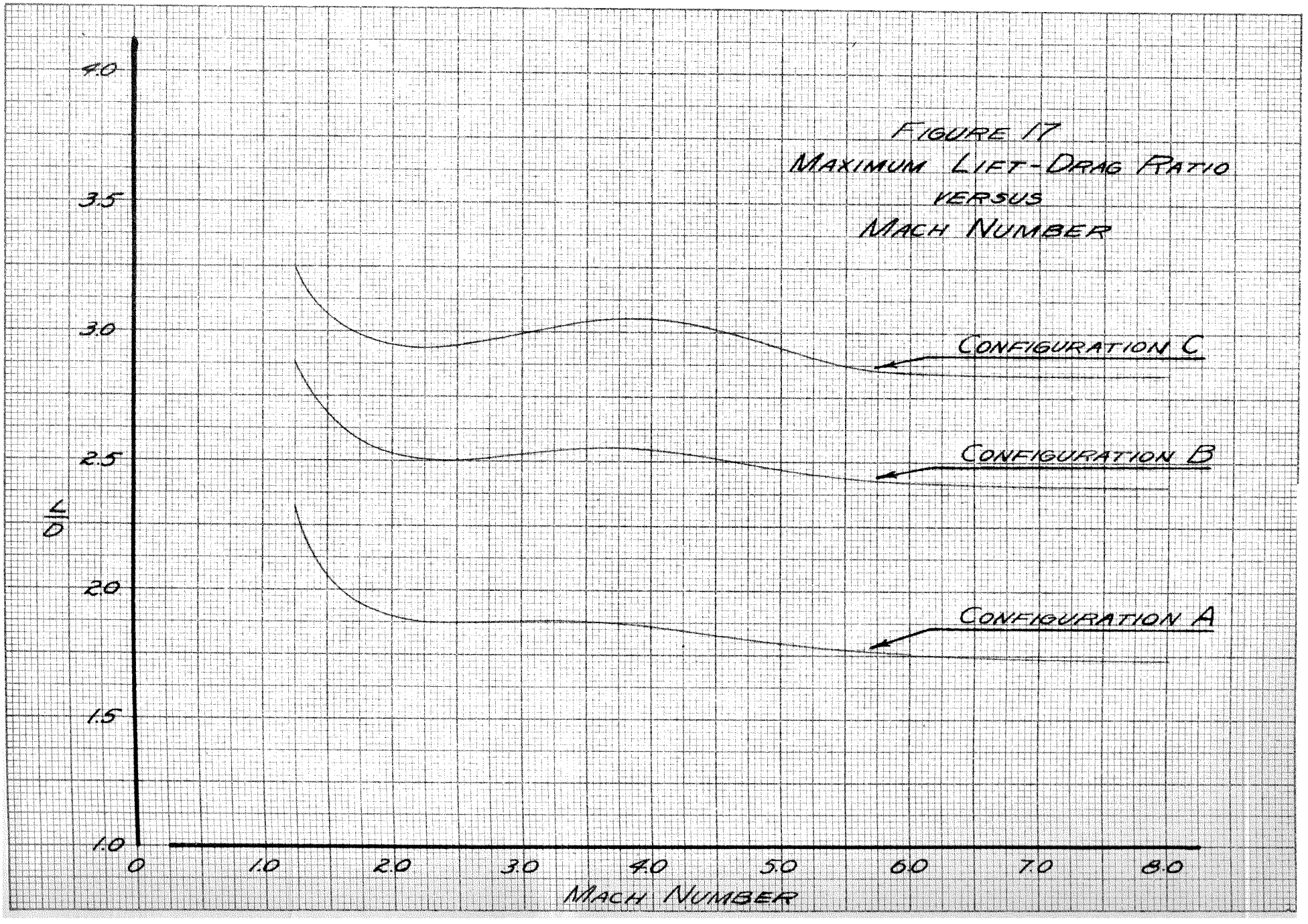
FIGURE 17
MAXIMUM LIFT-DRAG RATIO
VERSUS
MACH NUMBER
4.0
3.5
3.0
2.5
2.0
1.5
1.0
L/D
CONFIGURATION C
CONFIGURATION B
CONFIGURATION A
0
1.0
2.0
3.0
4.0
5.0
6.0
7.0
8.0
MACH NUMBER

FIGURE 18

LIFT - DRAG RATIO VERSUS MACH NUMBER

CONFIGURATION A

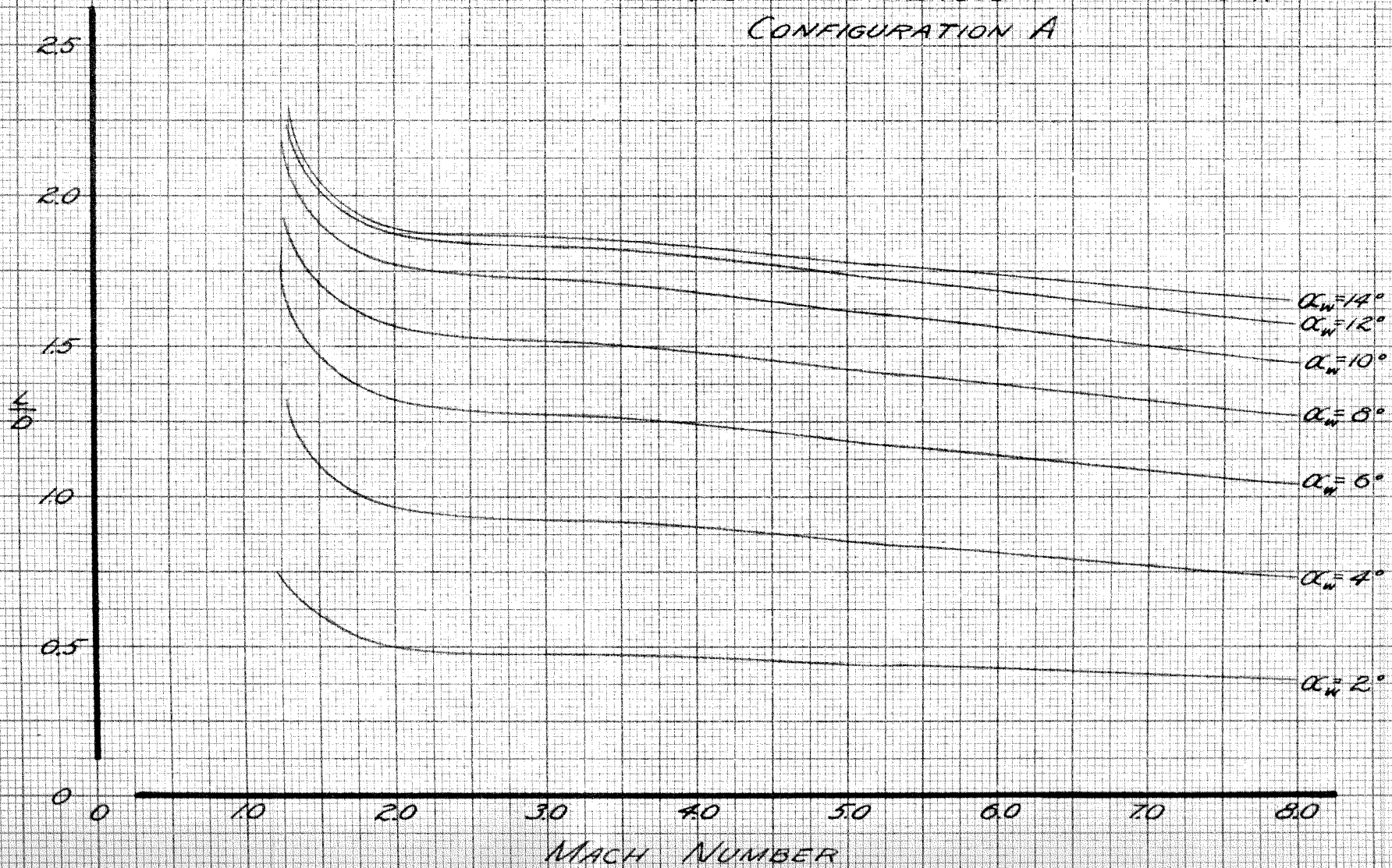

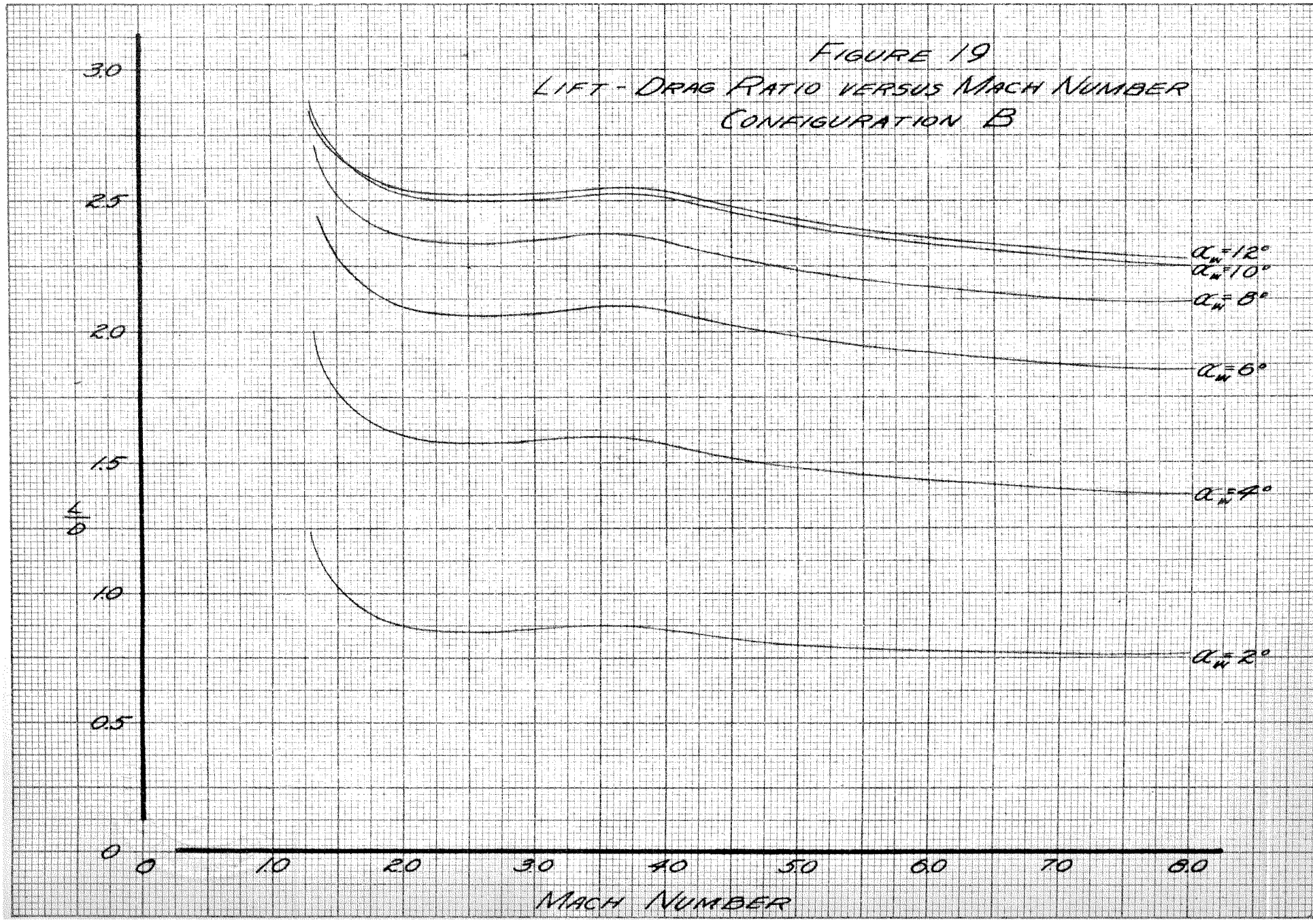
FIGURE 19
LIFT - DRAG RATIO VERSUS MACH NUMBER
CONFIGURATION B
3.0
2.5
2.0
1.5
1.0
0.5
0
L/D
0
1.0
2.0
3.0
4.0
5.0
6.0
7.0
8.0
MACH NUMBER
$\alpha_w = 12°$
$\alpha_w = 10°$
$\alpha_w = 8°$
$\alpha_w = 6°$
$\alpha_w = 4°$
$\alpha_w = 2°$

FIGURE 20
LIFT-DRAG RATIO VERSUS MACH NUMBER
CONFIGURATION C

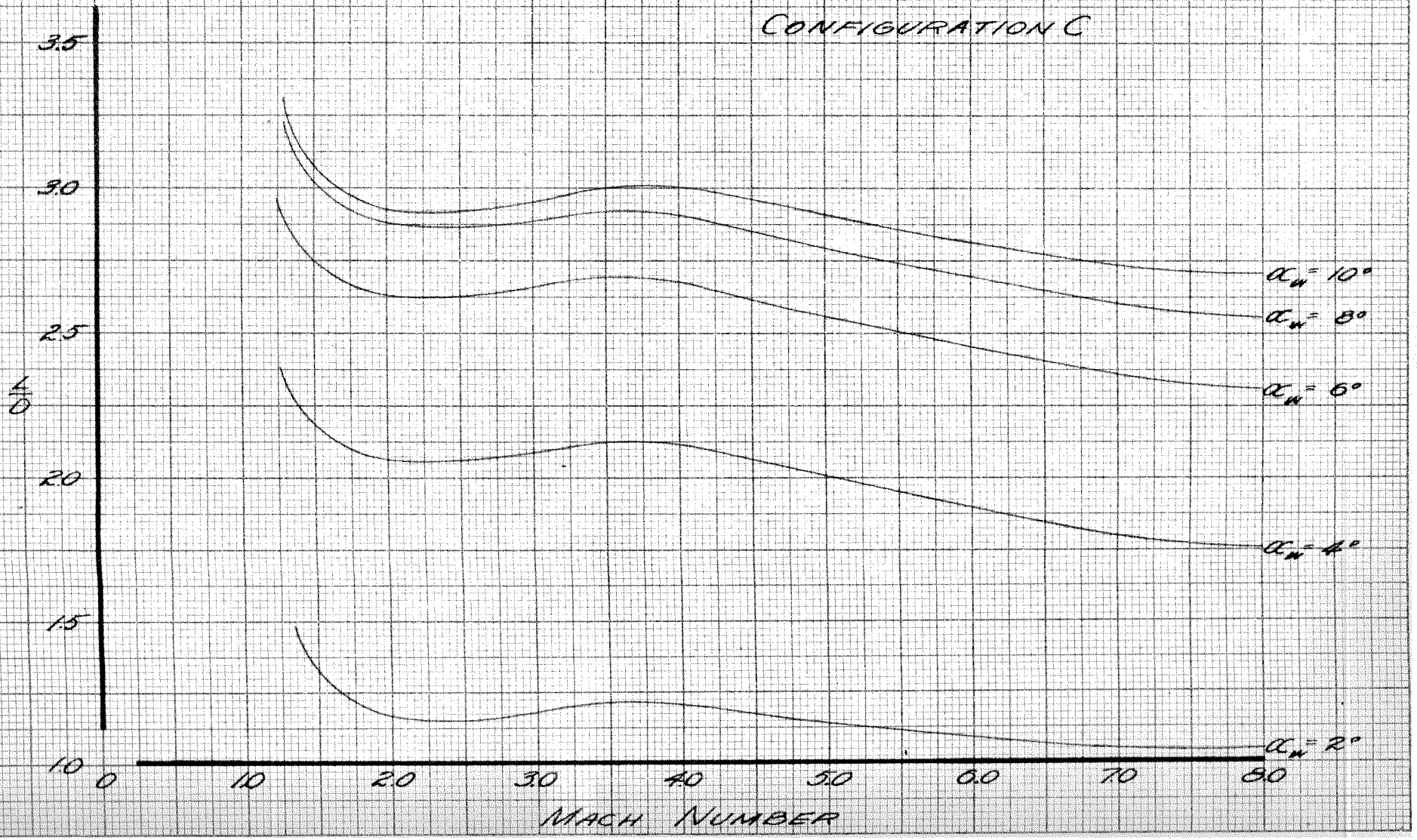

FIGURE 21
THRUST VARIATION WITH ALTITUDE

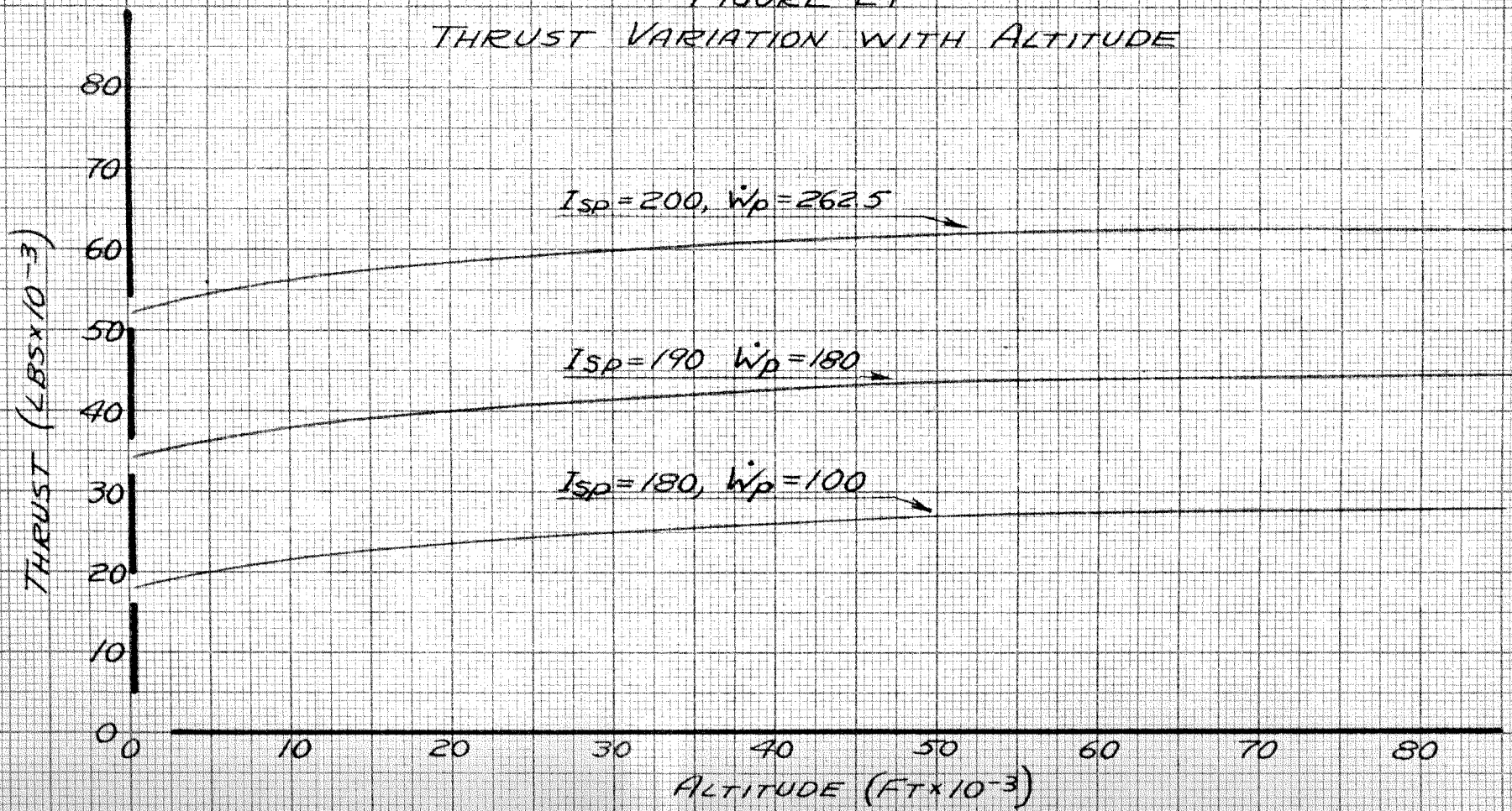

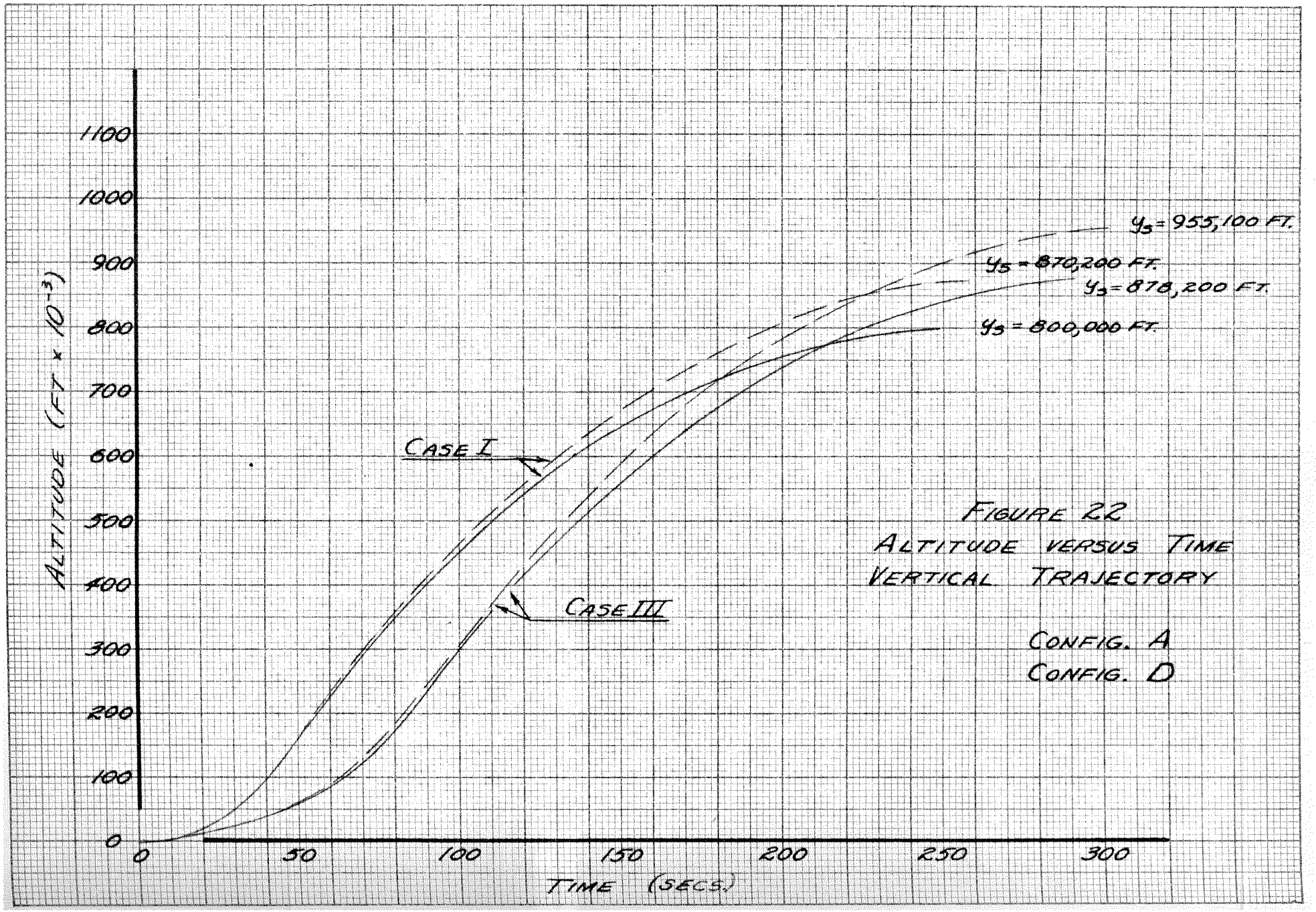

FIGURE 22
ALTITUDE VERSUS TIME
VERTICAL TRAJECTORY

CONFIG. A
CONFIG. D

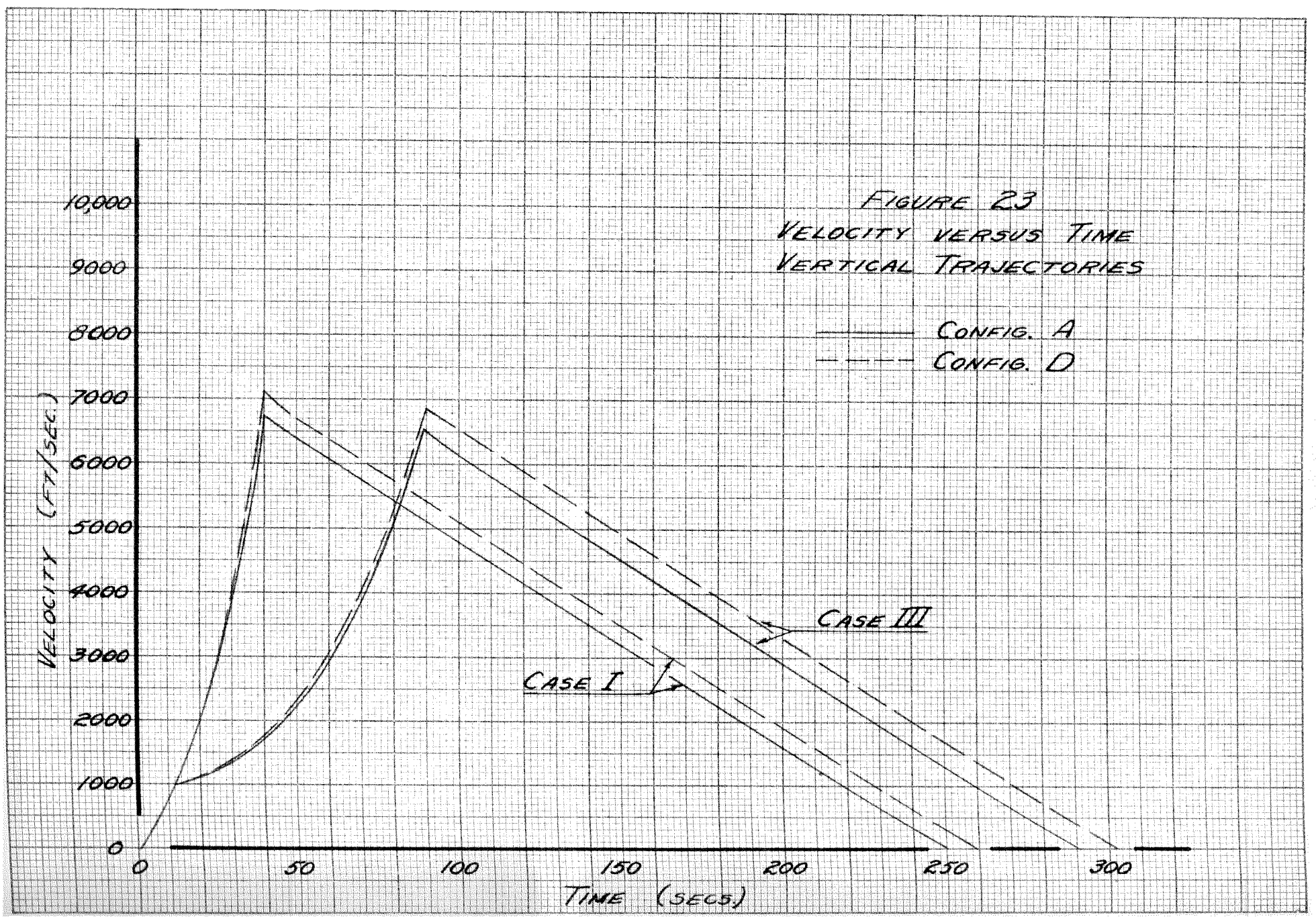
FIGURE 23
VELOCITY VERSUS TIME
VERTICAL TRAJECTORIES
CONFIG. A
CONFIG. D
CASE III
CASE I
VELOCITY (FT/SEC.)
10,000
9000
8000
7000
6000
5000
4000
3000
2000
1000
0
0
50
100
150
200
250
300
TIME (SECS.)

FIGURE 24
ALTITUDE VERSUS HORIZONTAL RANGE
CONFIGURATION A
CASE I